Med

LRG1 destabilizes tumor vessels and restricts immunotherapeutic potency
--Manuscript Draft--

Manuscript Number:	MED-D-20-00161R2
Full Title:	LRG1 destabilizes tumor vessels and restricts immunotherapeutic potency
Article Type:	Clinical and Translational Article
Keywords:	Leucine-rich α-2-glycoprotein 1, vascular normalization, tumor microenvironment, pericyte, cancer therapy, immunotherapy, vasculopathic, transforming growth factor β
Corresponding Author:	John Greenwood, PhD University College London Institute of Ophthalmology London, UNITED KINGDOM
First Author:	Marie O'Connor
Order of Authors:	Marie O'Connor
	David Kallenberg
	Carlotta Camilli
	Camilla Pilotti Pilotti
	Athina Dritsoula
	Rene Jackstadt
	Chantelle Bowers
	Angharad Watson
	Markella Alatsatianos
	Julia Ohme
	Laura Dowsett
	Jestin George
	Jack Blackburn
	Xiaomeng Wang
	Mahak Singhal
	Hellmut Augustin
	Ann Ager
	Owen Sansom
	Stephen Moss
	John Greenwood, PhD
Abstract:	Background: Vascular dysfunction contributes to the pro-oncogenic tumor microenvironment and impedes the delivery of therapeutics. Normalizing the tumor vasculature to reverse such deleterious effects has therefore become a therapeutic objective. We previously reported that the secreted glycoprotein, leucine-rich α-2-glycoprotein 1 (LRG1), contributes to pathogenic neovascularization by modifying TGFβ signaling. Here we investigate whether LRG1 is vasculopathic in tumors and whether its inhibition is therapeutically beneficial. Methods: Mouse tumor growth and vascular structure were analysed in subcutaneous and in genetically engineered mouse models in the presence and absence of Lrg1 . The effects of LRG1 antibody blockade as monotherapy, or in combination with cisplatin, adoptive T cells or an anti-PD1 antibody, on vascular function and tumor growth were investigated. Findings: In mouse models of cancer Lrg1 expression was induced in tumor

endothelial cells, consistent with an increase in protein expression in human cancers. The expression of LRG1 impacted on tumor progression as   Lrg1   gene deletion, or treatment with a LRG1 function-blocking antibody, inhibited tumor growth and improved survival. Inhibition of LRG1 increased endothelial cell pericyte coverage and improved vascular function resulting in enhanced efficacy of cisplatin chemotherapy, adoptive T-cell therapy and immune checkpoint inhibition (anti-PD1) therapy. With immunotherapy, LRG1 inhibition led to a significant shift in the tumor microenvironment from being predominantly immune silent (cold) to immune active (hot).

Conclusions: LRG1 drives vascular abnormalization and its inhibition represents a novel and effective means of improving the efficacy of cancer therapeutics.

Suggested Reviewers:	Elisabetta Dejana, PhD FIRC Institute of Molecular Oncology: Fondazione Istituto FIRC di Oncologia Molecolare elisabetta.dejana@ifom.eu Expert in vascular biology and cancer
	Christer Betsholtz Uppsala Universitet christer.betsholtz@igp.uu.se Expert in vascular biology and the role of the pericyte
	Robert Kerbel, PhD Sunnybrook Research Institute robert.kerbel@sri.utoronto.ca Expert in tumor vasculature
Opposed Reviewers:	
Additional Information:	
Question	Response
Datasets<p>Does your manuscript report new large-scale datasets?	
Standardized datasets<p>A list of datatypes considered standardized under Cell Press policy is available here. Does this manuscript report new standardized datasets?	No
Original Code<p>Does this manuscript report original code?	No

UCL INSTITUTE OF OPHTHALMOLOGY

Dr Elena Bellafante
Cell Press
50 Hampshire St., 5th Floor
Cambridge, MA 02139, USA

September 24th 2021

Dear Dr Bellafante

Re: Manuscript "LRG1 destabilizes tumor vessels and restricts immunotherapeutic potency" MED-D-20-00161

We are delighted to see that our paper has been accepted for publication and that there are no further modifications to be made. Please find uploaded all the documents as requested.

We have addressed all issues raised in points (a) - (e) in your acceptance letter.

We suggest a running title of: "Therapeutic targeting of LRG1 in cancer"

Finally, if possible, we would like to make the manuscript open access to comply with our funders requirements. Could you let us know how to proceed with this?

Yours sincerely

John Greenwood
Davson Professor of Biomedical Research

Steve Moss
Ashton Professor of Biomedical Research

Professor John Greenwood, UCL Institute of Ophthalmology, 11-43 Bath Street, London EC1V 9EL
Tel: +44 (0)20 7608 6858   Fax: +44 (0)20 7608 6810
Email: j.greenwood@ucl.ac.uk
www.ucl.ac.uk/ioo

Manuscript "LRG1 destabilizes tumor vessels and restricts immunotherapeutic potency" MED-D-20-00161

Response to reviewers

Reviewer #1:

O'Connor et al. described a role of Lrg1 during tumor progression. They proposed Lrg1 is an important therapeutic target, targeting of which would lead to both normalization of tumor vessel and activation of anti-cancer immunity. Through the impressive amount of experiments and experimental models, the authors provide high quality data and show that Lrg is an attractive novel molecule to target in cancer. Nevertheless, the following points still need to be addressed:

We thank this reviewer for a thorough, thoughtful and supportive review. We agree with most of the comments and the pertinent and interesting suggestions for further work. We believe, however, that much of this falls outside the scope and capacity of this study and would constitute a major investigation in its own right. Indeed, many of the suggestions are part of a substantial and ongoing in-house study that will form the basis of an extensive and in-depth assessment of the effect of LRG1 on the tumor immune microenvironment. We would like to emphasise that the main focus of this manuscript is the role of LRG1 on the tumor vasculature. The pleiotropic action of LRG1 makes this a rational approach.

Major comments:

1. *In Figures 1 and S1, the authors have shown the expression of Lrg1 in the normal and tumor tissues of mouse. Please check if it is possible to evaluate Lrg1 expression in the normal and tumor tissues of human.*

We have undertaken immunohistological evaluation for LRG1 in human tumors demonstrating its presence in the tumor mass and in vascular endothelial cells. We have also measured circulating levels of LRG1 in naïve cancer patients and normal controls and demonstrate significantly raised levels in the tumor-bearing patients. These data are now included in a new Figure 1.

Moreover, I suggest that the authors should assess whether Lrg1 expression is correlated with the prognosis of cancer patients, and then, compare it at different stages of tumor.

This is an important point and there are already a number of publications reporting that LRG1 is prognostic. As pointed out by reviewer 3 (point 2) some of these have been cited in the manuscript and are in the supplementary table. We have now cited all the relevant papers in the main text and removed the table. While further clinical studies would be corroborative, for us to conduct a clinical evaluation would lie outside the scope of this study and would constitute a separate independent piece of work.

2. *In Figure S4, altered gene expression in tumor microenvironment (TME) was observed*

based on the RNA-seq data. However, these genes might also be expressed in tumor cells, as well as stromal cells of TME. Therefore, I suggest the authors to further demonstrate the gene expression related to angiogenesis, endothelial mutation, and high endothelial venules (HEVs) in isolated tumor endothelial cells from various mice (Lrg-1 wild type, Lrg-1 knockout, and Lrg-1 WT treated with 15C4)?

We have now also added RNASeq data from endothelial cells isolated from B16 tumors +/- 15C4 treatment (now supplementary figure 3). As with whole tumor transcriptomic analysis this also revealed little change in the genes of interest. We also show elsewhere, by qPCR and immunohistochemistry, no HEV formation (Supplementary Fig. 7). As the primary question here was to establish what the effect 15C4 had we feel that, whilst investigating other treatment combinations would bring further insight, it would constitute a substantial additional study and fall outside the scope of this set of work.

3. *To validate the mechanism of action of cisplatin, I suggest the authors to assess the status of cell cycle arrest using flow cytometry.*

We feel that this is outside the scope of this study.

4. *In Figures 7 and 8, the authors have shown significant tumor growth inhibition in some mice through evaluating mean growth rate. Furthermore, to provide potential reasons, I suggest the authors to evaluate the induction of immunological memory by re-challenging tumor cells.*

We are unsure why any potential effects on T cell memory would impact on this primary tumor model response. Development of tumor-specific T cell memory would take at least 2 weeks to develop and hence would be unlikely to affect the growth of rapidly growing B16 and LLC tumors. Similarly, to critically evaluate a memory response to the primary tumor would require the development of memory prior to re-challenge with tumor which is not feasible in these models. Finally, staining for markers of memory cells on TILs would not necessarily demonstrate functionality. The focus of this study is the vasculature, and the potential effect of LRG1 on the immune system represents a substantial and on-going separate investigation.

5. *Most of the images in this article are clear and convincing. However, in Figure 8, it is hard to distinguish CD8 T-cells from the background. I suggest the authors to provide more representative images for this figure.*

We agree. This was due to the technical challenge of selecting a fixation condition that works with all three different antibodies. We concur that the CD8 stain is less than ideal and so now show improved images in Figure 7.

Also, I recommended to quantify various T-cells, such as CD8 T-cells, CD4 T-cells, and Tregs in this experiment.

We show infiltration of tumor-specific CD8$^+$ T cells but are not sure of the additional value of showing CD4 in this study. Whilst CD4 may be involved in tumor rejection one would need to look in a much more granular manner to establish the CD4 subsets

involved and their tumor antigen specificities and we believe this also lies outside the scope of this study.

6. *In Figure 8C, the authors have demonstrated an increase in the number of CD8+ T-cells within the tumor and that these are GzB+ activated T-cells. Please clarify whether these are tumor-specific T-cells or nonspecific bystander T-cells.*

To address this question, we would need to undertake tetramer staining to detect TCRs specific for tumor-restricted antigens and this does not work in tissue sections. This would require a new study involving FACS analysis. Whilst of interest, we feel that addressing these questions would require a much more in depth study to be meaningful, and this is something that we intend to do over the next few years.

7. *The authors have demonstrated that the genetic or pharmacological blockade of Lrg1 induces tumor vascular maturation. Please clarify if this process of vascular maturation prevents hematogenous metastasis of tumor cells to distant organs, such as the lungs or liver.*

This is an interesting question. The subcutaneous models employed do not allow for studying metastases as they reach ethical end-points before metastases are able to establish. To overcome that the primary tumor needs to be resected. We now include data showing LRG1 blockade reduces metastatic cancer (Figure 4). In a complimentary paper by our collaborators in Heidelberg (Singhal et al) we show that this effect is due to vascular niche priming. This paper is in press.

8. *Recently, VEGFR blockade was proven to enhance the efficacy of PD-1 blockade in many clinical trials. Since Lrg1 is a novel molecule that governs the tumor vascular phenotype and its efficacy as a monotherapy was moderate, I would like to see therapeutic efficacies of combining Lrg1 blockade with VEGFR2 blockade, or VEGFR2+PD-1 blockade. Please discuss whether these combinations would lead to enhanced tumor control and prolonged survival in tumor-bearing mice.*

We agree that this is an interesting question but would assert that to do this substantial additional work would neither confirm nor invalidate the combinatorial data presented. It would simply be an addition to the therapeutic regimens already presented. This will undoubtedly form the basis of future studies.

9. *The authors have proposed that Lrg1 may act as a potential target in tumor angiogenesis. To determine whether Lrg1 plays a non-redundant role in tumor angiogenesis, it would be important to examine its role in normal angiogenic vessels of adult mice. For instance, it should be verified if Lrg1 is important for wound healing (i.e., in WT versus KO mice).*

We show in the Nature paper (cited) that LRG1 is redundant for developmental angiogenesis as the KO mice have no overt phenotype. We have shown in a recently published paper that LRG1 may play a "physiological" role in wound healing (Lui et al., 2020) which is cited. This is also supported by an additional recent paper (Gao et al 2020) that we also now cite.

10. *The authors demonstrated a correlation between Lrg1 expression and angiogenesis. Furthermore, they suggested that Lrg1 may be involved in lymphoangiogenesis.*

Nowhere in the manuscript do we say that LRG1 is involved in lymphangiogenesis. We have stained for Lyve1 but this was negative in the B16 tumours in all settings. We could show this negative data if required.

To validate the effects of Lrg1 on cancer metastasis to lymph nodes, I suggest they should also evaluate the expression of Lrg1 in lymphatic vessels.
Furthermore, it is important to address the following question: How does Lrg1 expression in blood endothelial cells affect cancer metastasis to lymph nodes?

We didn't investigate metastatic spread to the lymph nodes so we are uncertain why we need to validate it. The B16 subcutaneous tumor model is not thought to metastasise via the lymphatics. Moreover, we believe this to be tangential to the study as it addresses the role of LRG1 in tumor dissemination from the primary tumor. This has been addressed in the in press *Sci Trans Med* paper of our collaborators mentioned earlier.

Minor issues

Reviewer #1: *1. On page 6, line 3, the authors have mentioned the previous work, demonstrating that Lrg1 knockout leads to a reduction in the size of neovascular lesions. To better comprehend the effects of Lrg1 gene deletion, the authors need to cite the appropriate reference here.*

We cite this paper but have cited it again here (Wang et al Nature 2013).

2. *On page 6, line 8, the authors have indicated tumor growth of vilCreER Apcfl/+ in Fig. 1D. However, this result is presented in Fig. 2D. Therefore, the authors should change Fig. 1D to 2D in the text accordingly.*

Thanks for noting this. This has been corrected.

Reviewer #2:

In this manuscript, O'Connor and colleagues show that genetic or antibody-mediated inactivation of LRG1, a secreted glycoprotein that promotes dysfunctional vascular growth via TGFB signaling, normalizes tumor blood vessels and facilitates immune-mediated anti-tumoral responses in several cancer models.

General assessment

Reference #1 (Nature, 2013) showed a role for TGFB in LRG1-induced vascular dysfunction in models of pathological ocular angiogenesis. In the current study, the authors examined the effects of inactivating LRG1 in mouse tumor models. While the manuscript does not offer new molecular insight into how exactly LRG1 inactivation promotes vascular normalization and immune cell trafficking in tumors, the data are interesting and timely, largely compelling, transparently reported, and translationally relevant. Specific strengths of the work are the careful documentation of the vascular and immune-cell phenotypes regulated by LRG1 and the translational potential of the data, which involve both genetic and pharmacological evidence of the benefits of targeting LRG1 in distinct tumor models, including genetically engineered mice.

I should disclose that I had reviewed an earlier version of this manuscript. I feel that the current submission addresses my general concerns with the earlier version of the manuscript (e.g., by including discussion of the potential advantages of LRG1 blockade compared to direct therapeutic targeting of the TGF β superfamily; analysis of the potential role of HEV formation in improved T-cell trafficking after adoptive cell therapy; better contextualization of the data; etc.). Also, specific technical points have been resolved. In my opinion, the manuscript is now ready for publication.

We are most grateful for this reviewers' positive comments.

Reviewer #3:

1. *Through RNAseq analyses, authors conclude that no transcripts involved in angiogenesis or endothelial cell metabolism are significantly changed and suggest that the effects may be post-transcriptional (or post-translational). It would improve the story if the phenotypes observed were followed through from this perspective, in order to provide some clarity as to on which parameters LRG1 may be exerting an impact. Changes in the receptors (such as TGFb, endoglin and other downstream effectors could have been explored, even in tumour models where LRG1 was not directly overlapping with EC).*

This is a valid comment albeit extremely challenging. We have now included some western blot analysis of tumor tissue comparing control with 15C4 treatment and reveal some changes to TGFbeta canonical and non-canonical signaling pathways. There are limits to what can be interpreted here but what it does illustrate is that blockade of 15C4 alters the signalome of the tumor mass. These data are presented in supplementary figure 4.

2. *Expression of LRG1 in malignant tissues was confirmed and compiled in a comprehensive table, demonstrating a correlation and a diagnostic marker for multiple malignancies, and as mentioned above, with vascular dysfunction. Curiously, only the two subcutaneous models (LLC and B16-F0) showed co-localization of LRG1 and endothelium.*

In addition to showing co-localization of LRG1 and endothelium in the subcutaneous models we also did report on colocalization in the endothelium of the GEMM tumours. This was originally shown in Figure 1D. It is now shown in Figure 1I. We additionally show Lrg1 expression in the metastatic tumor vessels (Figure 1J).

These are the two least physiological models, and the subcutaneous environment is rather unique in that it does not really recapitulate any human cancer microenvironment. Also, authors inject 1x10^6 cells, a number that would result in a very artificial tumor when compared to spontaneous cancer models or implants with lower cell number. This can, and very likely does, influence how these tumors progress and respond.
It stands to reason to question whether their observations are of primary relevance to their models; and this should be considered in the rationale for the remainder of the paper, where only these two models are scrutinized further (with particular emphasis on melanoma towards the end).

We accept the limitations of this (and indeed all) tumor models. To strengthen the message, we have now included an additional study investigating the combination of 15C4 with anti-PD1 in the highly refractory LLC tumor model. This is presented in Supplementary figure 7.

3. *The authors explore and demonstrate that tumors significantly regress using combination therapies that include LRG1 inhibition and chemotherapy, adoptive transfer and PD1 blockade, but only in the melanoma model. They conclude that, in a mechanism independent of HEV, tumors can become more immunogenic and thus more responsive to immunotherapy, in the absence of LRG1. However, once again, it is not clear why. Increased perfusion, or increased/more successful recruitment of T-cells?*

We presented data that showed LRG1 antibody blockade increased vascular perfusion (original Fig 5) and an increase in T cell recruitment (original Figs 7, 8 and supplementary Fig 9). To ascertain what is responsible for the increase in infiltration is the subject of future studies.

What is happening in the other LRG1-positive tumour models? Even the subcutaneous LLC model? If LRG1 is demonstrably present in all tumour models, what happens to tumor progression and survival in non-melanoma malignancies?

As mentioned above we now include positive data from the LLC model which is highly resistant to checkpoint inhibition.

4. *Did the authors consider looking into metastatic dissemination? Both melanoma and LLC tumours should have disseminated to the lung, so it would be interesting to see if the LRG1 blockade had any influence in disseminated disease, a very serious concern for melanoma patients.*

Metastases of these tumors do not establish by the time the animals reach their humane end point. To overcome this limitation resection of the primary tumor is required. We now present data using this model that shows LRG1 inhibition attenuates metastatic seeding (Figure 4). This is explored in detail in our collaborators study that is in press and referred to in the latest manuscript (Singhal et al 2021 in press).

Minor comments:

* Authors use a-SMA and NG2 interchangeably for pericyte staining, when a-SMA will also stain VSMC; possibly best to identify in all cases as perivascular mural cells?

We agree and have changed this as suggested.

* *Figure 2 - survival and tumor growth curves show minimal difference... does this really represent a survival advantage? It would appear that the tumors in the KO mice would eventually catch up... is 15 days enough for this comparison?*

We would argue that this is a significant effect. In the B16 and LLC tumors at termination the reduction versus controls is 44% and 46% respectively. The experiments went as far as was permissible under our Government animal licence. Indeed, the value is an underestimate as we have to remove animals meeting the humane end point which skews it against showing treatment benefit. Consequently, the tumor size would be much larger in the control group if they were allowed to continue.

* *Figure 3 - vessel size refers to cross-sectional area. Possibly better labelled as vessel diameter?*
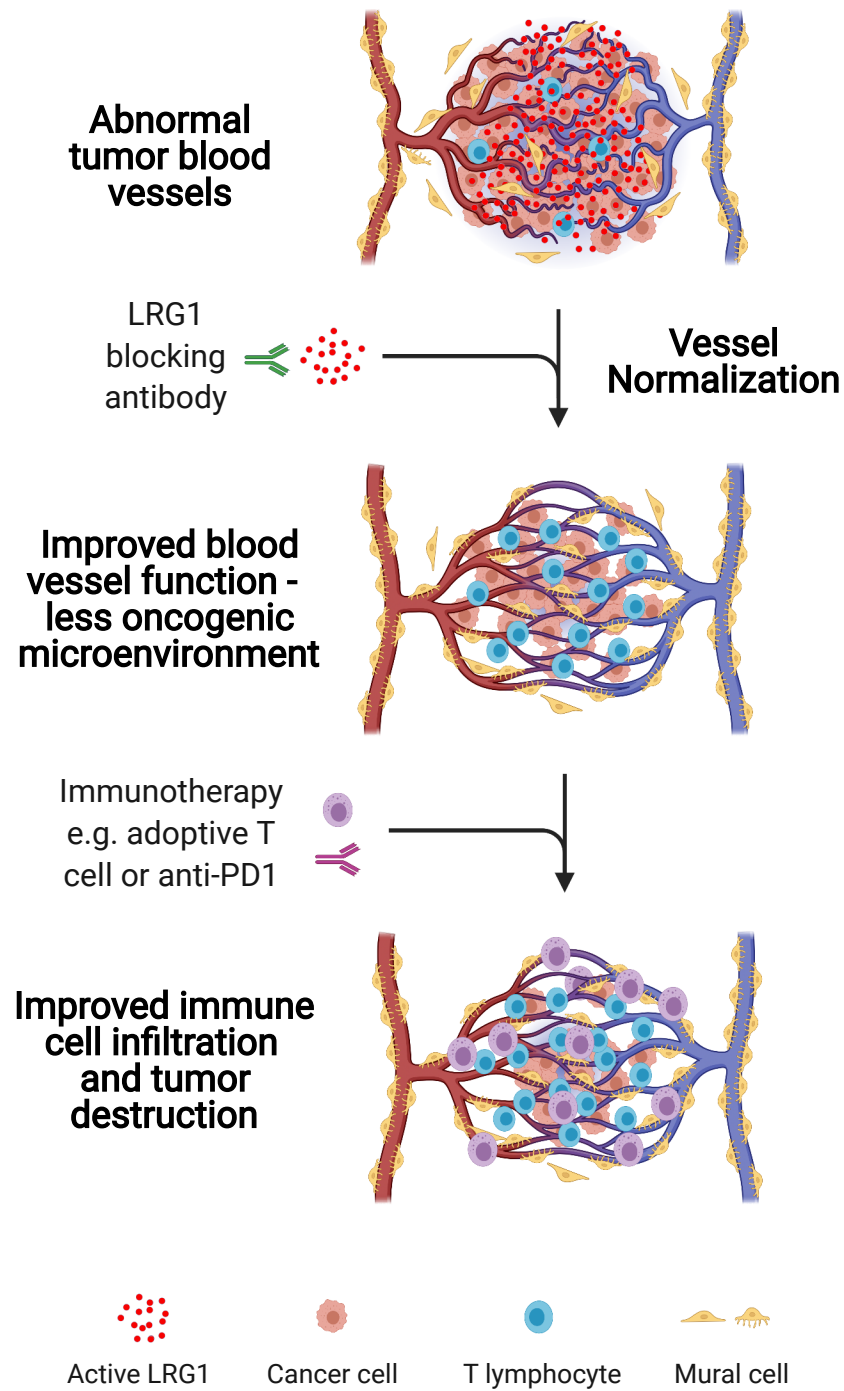
These are separate parameters and cross-sectional area is correct. We avoid diameter because vessels are sectioned through random orientation.

* *Figures 7 and 8 have the same title*

This has been amended.

Supplemental figures are showing tumor growth over time in response to multiple combination therapies; measurements stop at days 15-16 (Supplemental Figure 6, 7 and 10), which seem a little early. For experiments in figures 8 and 9 these measurements are carried out for 30 and 40-42 days, respectively... what is the rationale for these discrepancies?

The shorter time was because when the first B16F0 tumour animals reached the humane end point all mice were culled on the same day for histology to make a legitimate comparison. The tumour growth rates in Supp Figs 8 and 9 were due to different B16 cells being used (B16-F10 as opposed to B16-F0) and were also transfected with the surrogate tumor antigen, all of which altered their in vivo growth kinetics.

Graphical Abstract

Abnormal tumor blood vessels

LRG1 blocking antibody

Vessel Normalization

Improved blood vessel function - less oncogenic microenvironment

Immunotherapy e.g. adoptive T cell or anti-PD1

Improved immune cell infiltration and tumor destruction

Active LRG1   Cancer cell   T lymphocyte   Mural cell

LRG1 destabilizes tumor vessels and restricts immunotherapeutic potency

Marie N. O'Connor[‡1], David M. Kallenberg[‡1], Carlotta Camilli[1], Camilla Pilotti[1], Athina Dritsoula[1], Rene Jackstadt[2], Chantelle E. Bowers[1], H. Angharad Watson[3], Markella Alatsatianos[3], Julia Ohme[3], Laura Dowsett[1], Jestin George[1], Jack W.D. Blackburn[1], Xiaomeng Wang[1], Mahak Singhal[4,5], Hellmut G. Augustin[4,5], Ann Ager[3], Owen J. Sansom[2,6], Stephen E. Moss[*†1] and John Greenwood[*†§1]

[1]Institute of Ophthalmology, University College London, London, SE5 8BN, UK
[2]Cancer Research UK Beatson Institute, Glasgow, G61 1BD, UK
[3]Division of Infection and Immunity, School of Medicine and Systems Immunity University Research Institute, Cardiff University, Cardiff, CF14 4XN, UK
[4]Division of Vascular Oncology and Metastasis, German Cancer Research Center (DKFZ-ZMBH Alliance), Heidelberg, Germany
[5]Department of Vascular Biology and Tumor Angiogenesis, European Center for Angioscience (ECAS), Medical Faculty Mannheim, Heidelberg University, Mannheim, Germany
[6]Institute of Cancer Sciences, University of Glasgow, Glasgow, G61 1QH, UK.

[‡] These authors contributed equally
[†] These authors contributed equally
[§] Lead contact: John Greenwood

*Correspondence: j.greenwood@ucl.ac.uk (J.G.) or s.moss@ucl.ac.uk (S.E.M.)

ABSTRACT

Background: Vascular dysfunction contributes to the pro-oncogenic tumor microenvironment and impedes the delivery of therapeutics. Normalizing the tumor vasculature to reverse such deleterious effects has therefore become a therapeutic objective. We previously reported that the secreted glycoprotein, leucine-rich α-2-glycoprotein 1 (LRG1), contributes to pathogenic neovascularization by modifying TGFβ signaling. Here we investigate whether LRG1 is vasculopathic in tumors and whether its inhibition is therapeutically beneficial.

Methods: Mouse tumor growth and vascular structure were analysed in subcutaneous and in genetically engineered mouse models in the presence and absence of *Lrg1*. The effects of LRG1 antibody blockade as monotherapy, or in combination with cisplatin, adoptive T cells or an anti-PD1 antibody, on vascular function and tumor growth were investigated.

Findings: In mouse models of cancer *Lrg1* expression was induced in tumor endothelial cells, consistent with an increase in protein expression in human cancers. The expression of LRG1 impacted on tumor progression as *Lrg1* gene deletion, or treatment with a LRG1 function-blocking antibody, inhibited tumor growth and improved survival. Inhibition of LRG1 increased endothelial cell pericyte coverage and improved vascular function resulting in enhanced efficacy of cisplatin chemotherapy, adoptive T-cell therapy and immune checkpoint inhibition (anti-PD1) therapy. With immunotherapy, LRG1 inhibition led to a significant shift in the tumor microenvironment from being predominantly immune silent (cold) to immune active (hot).

Conclusions: LRG1 drives vascular abnormalization and its inhibition represents a novel and effective means of improving the efficacy of cancer therapeutics.

INTRODUCTION

Angiogenesis is notably different in development and disease, with the former producing an organized, stable and functional vascular network, and the latter being typically disorganized and dysfunctional. Yet vascularization in both settings is driven by many of the same molecules, such as vascular endothelial growth factor (VEGF). Why vessels fail to grow in a patterned and functional manner in most disease settings remains poorly understood but points to the potential involvement of novel pathogenic factors that corrupt physiological angiogenesis. We, and others, have previously shown that in vascular pathology of the retina[1] and kidney[2] the secreted glycoprotein LRG1 is induced and promotes dysfunctional vessel growth through modifying endothelial cell TGFβ signaling. Importantly, deletion of *Lrg1* in mice did not impact on developmental angiogenesis with the mice exhibiting no overt phenotype[1]. These observations suggest that in disease LRG1 might be a contributing pathogenic factor responsible for preventing the development of physiological vessels and thus play a role in the vascular dysfunction that is prevalent in cancer.

The formation of new blood vessels has long been recognized as an essential feature of tumor expansion, survival and metastatic spread[3,4]. Consequently, targeting of key pro-angiogenic signaling molecules, most notably VEGF through blocking antibodies such as bevacizumab, to limit vascular growth or to regress existing vessels has become an established therapeutic regimen. Whilst such approaches have met with some success, resulting in an increase in progression-free survival in certain cancers, they have had little impact on overall survival rate. As in other diseases, cardinal features of tumor vessels are that they are poorly perfused, leaky and hemorrhagic; characteristics believed to be due in part to the failure of vessel maturation. These abnormal features result in a hypoxic pro-oncogenic tumor microenvironment (TME) that promotes malignancy and metastatic spread, impairs beneficial immune responses, and limits the efficacy of systemically administered drugs and immunotherapeutics[5,6]. Counter to the original rationale of blocking

neovascularization, therefore, an alternative strategy has emerged which aims to normalize

the vasculature and render the microenvironment more conducive to tumor destruction[7,8]. In

pursuit of this objective, various approaches have been tested including the use of anti-

VEGF drugs delivered at a lower dose than that required to prevent, or ablate,

neovascularization[9]. This tactic has led to some improvement in the delivery of cancer

therapeutics[10,11] but the timing and dosage remain problematic, especially as the window of

opportunity with anti-VEGF drugs may be transient[10,12,13]. To overcome this limitation other

vascular modifying approaches have been explored, either as monotherapy or in conjunction

with existing anti-VEGF drugs[14-22]. These studies have demonstrated that sustained vascular

normalization can be achieved, at least in the experimental setting, and validate the potential

utility of these strategies in enhancing the efficacy of current standard of care and emerging

treatments. Moreover, these studies also highlight the importance of crosstalk between the

vasculature and the immune system in establishing a favorable therapeutic milieu[19,23-26]. In

particular, it has been shown that vascular normalization strategies combined with

checkpoint inhibition result in the formation of high endothelial venule (HEV) characteristics

within the tumor vasculature that help promote the recruitment of effector T cells[14]. It is clear,

therefore, that there is much that we still need to understand about the contribution that the

vasculature makes to tumor progression and in so doing reveal new potential therapeutic

targets.

The discovery that LRG1 is associated with abnormal vessel growth in various diseases[1,2]

raises the possibility that this secreted glycoprotein contributes to abnormal tumor vessel

growth. Consistent with this hypothesis, studies have shown *LRG1* to be induced in many

carcinomas, and there is growing evidence that raised blood LRG1 levels alone, or in

combination with other biomarkers, correlate with increased tumor load and poor

prognosis[27-39]. Such data strongly implicate LRG1 in the pathogenesis of cancer and provide

a rationale for further investigation. In this study, therefore, we aimed to establish whether

LRG1 impacts on tumor vessel structure and function and crucially the implications of this on

therapy. We show that LRG1 affects vessel growth, structure and function, establishing it as a significant vascular destabilizing factor. By deleting *Lrg1,* or blocking its function with a targeted antibody, we observe reduced tumor growth, and demonstrate that tumor vessels exhibit a more physiological configuration with improved pericyte coverage. The ramifications of vessel normalization brought about by LRG1 blockade were further investigated and revealed enhanced efficacy when combined with cytotoxic and immunotherapeutic strategies. These data provide evidence that blockade of LRG1 in cancer offers a novel approach to vascular normalization and in doing so, potentiates the efficacy of current and emerging therapies.

RESULTS

LRG1 expression is increased in human cancer patients

Under normal conditions LRG1 is expressed predominantly by the liver but in cancer there is strong evidence that its expression is significantly induced[27-39]. To confirm these findings LRG1 protein was examined by immunohistochemistry in human lung, prostate and breast carcinomas, with all three exhibiting high expression compared to adjacent normal appearing tissue or normal control tissue (Figure 1A, B and C). We also observed expression of LRG1 in peritumoral endothelial cells (Figure 1D). Having corroborated tumor expression of LRG1 we next determined, as previously reported, whether various cancer types were also associated with raised circulating blood levels. In serum collected from treatment-naïve patients with Grade III and above colorectal adenocarcinoma, pancreatic adenocarcinoma and squamous cell lung carcinoma, circulating levels of LRG1 were found to be significantly increased above normal circulating levels (Figure 1E). These data support the prevailing view that LRG1 may contribute to tumor progression.

***Lrg1* deletion reduces experimental tumor growth and increases survival**

To complement the data on LRG1 expression in human cancer, we next examined *Lrg1*

expression in the syngeneic B16-F0 mouse melanoma and Lewis lung carcinoma (LLC)

subcutaneous graft models, the KPC model of pancreatic ductal adenocarcinoma (PDAC)

(*LSL-Kras$^{G12D/+}$; LSL-Trp53$^{R172H/+}$; Pdx-1-Cre*), the *Apc$^{Min/+}$* and the *vil^{CreER} Apc$^{fl/+}$* models of

colorectal cancer (CRC). *Lrg1* transcript was detected within the tumors of all models (Figure

1F-H). In B16-F0 and LLC tumors, *Lrg1* expression appeared to be restricted mostly to

vessels (Figure 1F) whereas in intestinal adenomas and PDAC, *Lrg1* expression was also

highly upregulated in the neoplasm compared to normal tissue (Figure 1G,H. Supplementary

Figure 1A,B). Consistent throughout the different cancer models *Lrg1,* which is not

detectable in normal blood vessels, was induced in endothelial cells but not observed in

αSMA$^+$ perivascular mural cells (Figure 1I). We next investigated whether *Lrg1* gene

expression was also increased in metastatic tumor vessels. Vessels from LLC lung

metastases (Figure S1C) exhibited a strong induction of *Lrg1* compared with normal lung

vessels where the expression was barely detectable (Figure 1J; Figure S1D). Overall, these

observations align with our human data and previous reports[27-39], and raise the possibility

that local secretion of LRG1 may impact on the tumor microenvironment of primary and

metastatic tumors and, in particular, through both autocrine and paracrine signaling, on

vascular function.

Our previous work demonstrated that *Lrg1* knockout, or functional blockade with an

antibody, reduced the size of neovascular lesions in models of age-related macular

degeneration and ocular hypoxia[1]. We therefore examined the effects of *Lrg1* gene deletion

on tumor growth and survival across a range of syngeneic and genetic models. In the B16-

F0 and LLC subcutaneous tumors, tumor growth was significantly reduced in *Lrg1$^{-/-}$* mice

compared to WT controls (Figure 2A,B; Figure S2A,B), with a decrease in final tumor volume

at the termination end-point of 44% and 46%, respectively. Consistent with these

observations, the *Apc$^{Min/+}$* (Figure 2C) and *vil^{CreER} Apc$^{fl/+}$* (Figure 2D) mice also exhibited a

significantly enhanced survival rate on the *Lrg1$^{-/-}$* background. In both colorectal models

there was a trend towards a reduced tumor number in *Lrg1*^{-/-} mice that reached significance in the colon and small intestine in the *Apc*[Min/+] and *vil*[CreER] *Apc*^{fl/+} mice respectively (Figure 2E,F). We next investigated whether knockout of *Lrg1* affected the survival of KPC pancreatic ductal adenocarcinoma (PDAC) tumor-bearing mice[40]. As with the other models, *Lrg1*^{-/-} KPC mice exhibited a significantly enhanced survival rate compared to *Lrg1*^{+/+} mice (Figure 2G). These results demonstrate that deletion of *Lrg1*^{-/-} in a number of different tumor models improves outcome and supports the hypothesis that LRG1 is pro-oncogenic.

Lrg1 deletion results in tumor vessel normalization

To ascertain if reduced tumor size and enhanced survival in *Lrg1*^{-/-} mice correlated with changes in vascularization we measured the percentage of vessel area in each tumor type. No difference in total vessel area between wild type and *Lrg1* knockout mice was observed across the different models (Figure 3A,B Figure S2C). There was only a modest reduction in the number of vessel profiles per unit area in the B16-F0, LLC and KPC mice on the *Lrg1*^{-/-} background, but a striking increase in the size of individual vessels (Figure 3B,C). Due to the planar orientation of the tumor vasculature in the *Apc*[Min/+] models, comparable analysis of vessel density was not possible. Nonetheless, our observations that endothelial cells express the *Lrg1* gene in a pathological setting and that tumor vessels lacking *Lrg1* tend to be larger, raise the possibility that LRG1 impacts tumor vascularization.

The observed loss of small vessels, with a concomitant increase in larger vessels, is a characteristic associated with vessel normalization[13] and suggests that the presence of LRG1 may impair vessel maturation. Pericyte coverage and basement membrane deposition are additional features associated with vessel stabilization and maturation[41], and failure of these processes is known to contribute to vessel dysfunction[42]. We therefore investigated whether the absence of LRG1 affects this critical relationship. Using NG2 and/or αSMA as markers of mural cells, we observed that *Lrg1* deletion in the B16-F0, *Apc*[Min/+] and *vil*[CreER] *Apc*^{fl/+} models was associated with increased mural cell coverage of endothelial cells (Figure

3D,E). Whilst a similar trend was observed in the LLC and the KPC models, this did not reach significance. Similarly, vessels from B16-F0, $Apc^{Min/+}$ and $vil^{CreER} Apc^{fl/+}$ tumors, but not those from the LLC or KPC tumors, also exhibited increased basement membrane association (Figure 3F; Figure S2D). In further support of the observation that LRG1 depletion improves vascular structure, scanning electron micrographs of B16-F0 tumors from $Lrg1^{-/-}$ mice revealed a reduction in the amount of intraluminal membranous inclusions (Figure 3G), a recognized feature of abnormal tumor vessels[43]. These data indicate that not only does $Lrg1$ knockout impact on tumor size and survival, but its loss is also associated with the acquisition of a more normal vascular appearance.

LRG1 antibody blockade replicates *Lrg1* deletion and results in improved vascular function

Having demonstrated that deletion of $Lrg1$ influences tumor growth, we next asked whether this could be phenocopied by inhibiting the activity of LRG1 in wild type mice with a LRG1 function-blocking antibody. B16-F0 tumor-bearing mice, which exhibited robust effects of $Lrg1$ deletion and which are generally considered to respond poorly to therapeutic intervention, were treated intraperitoneally with 15C4, a LRG1 function-blocking monoclonal antibody[44]. As with $Lrg1^{-/-}$ mice, LRG1 antibody blockade resulted in a similar reduction in tumor volume of 39% at the experimental endpoint (Figure 4A, Figure S2E). As antibody blockade of LRG1 impacts on primary tumor growth we next investigated its effect on the LLC tumor metastasis model. Metastasis-bearing mice were treated perioperatively with 15C4 (Figure S1C) resulting in a significant improvement in survival (Figure 4B), showing that LRG1 antibody blockade not only replicates the therapeutic effect of $Lrg1$ knockout on primary tumor growth but also impacts on metastatic cancer.

We then assessed whether antibody blockade changes vascular function in primary B16-F0 tumors. As observed in $Lrg1$ knockout mice, 15C4 treatment of B16-F0 tumor-bearing mice resulted in a decrease in vessel density, an increase in vessel size (Figure S2F), and an

9

increase in mural cell association with tumor vascular endothelial cells (Figure 4C).

However, the increase in basement membrane coverage was not significant (Figure S2G).

These data show that inhibition of LRG1 largely recapitulates the impact of *Lrg1* genetic

deletion in B16-F0 tumors, resulting in a more physiological vascular configuration that may

be associated with vessel stabilization and improved vascular function.

To test this assertion, we examined whether inhibition of LRG1 leads to enhanced tumor

vessel perfusion. Using a systemically delivered fluorescent lectin tracer to mark perfused

vessels, and an antibody to decorate all endothelial cells in tissue sections, we observed a

significant increase in the percentage of perfused B16-F0 tumor vessels in mice treated with

15C4 (Figure 4D). Moreover, this increase in vascular patency was associated with a

significant reduction in tumor hypoxia (Figure 4E). Another feature of vascular normalization

is reduced vascular permeability through the stabilization of endothelial cell junctions. The

adherens junction protein VE-cadherin regulates vascular endothelial cell junction integrity

and its enhanced expression is associated with a reduction in vascular leakage[45]. In 15C4

treated mice we observed a significant increase in the intensity of staining for endothelial

VE-cadherin (Figure 4F) consistent with improved barrier integrity. In addition, we noticed a

reduction in tumor vessel permeability as indicated by limited diffusion of Hoechst dye from

perfused (lectin+) vessels (Figure 4G). Vascular normalization also resulted in a small but

non-significant increase in CD3+ T cells (Figure 4H). Taken together, these data indicate that

LRG1 blockade improves vascular function and in so doing confirms LRG1 both as an

angiopathic factor and potential therapeutic target in tumors.

To investigate whether *Lrg1* knockout or LRG1 blockade alters the expression of key

signaling axes genes involved in either vascular maturation or destabilization, we undertook

RNASeq analysis of B16-F0 tumor samples from *Lrg1* knockout and WT mice and from

endothelial cells isolated from either 15C4 or IgG control treated B16-F0 tumors.

Accordingly, we investigated signature genes for the receptor-ligand pathways of VEGF,

angiopoietin (ANGPT), platelet derived growth factor (PDGF), TGFβ, sphingosine 1-phosphate (S1P), Notch, Wnt, Hedgehog, fibroblast growth factor, ephrin and apelin in tumor tissue and in isolated tumor endothelial cells (Figure S3). We also investigated the expression of key glycolytic pathway genes that have been associated with angiogenesis[46] and vascular dysregulation[47]. No significant differences were observed except for an increase in the knockout mouse tumors of the flow-sensitive transcription factor Krüppel-like factor 2 (*Klf2*) (Figure S3A) and in the 15C4 treated endothelium a decrease in the type 1 transmembrane family member *Notch2* (Figure S3B).

These data suggest that the dysregulation of these genes may not be responsible for the LRG1 effects, or that LRG1 may operate post-translationally by impacting on signaling mechanisms. To address the latter possibility, we investigated whether LRG1 inhibition altered the phosphorylation status of intermediate signaling components associated with the canonical and non-canonical TGFβ pathways. Using whole tumour protein lysates, we observed that the expression of the phosphorylated kinases AKT and ERK1/2, but not of JNK or p38, was significantly reduced in 15C4 treated mice (Figure S4A). Whilst this does not reveal the cell source or the upstream origin, it is consistent with an effect on non-Smad mediated TGFβ signaling and demonstrates that 15C4 is impacting on the tumor signaling environment. Moreover, we also observed a significant reduction in the phosphorylation of SMAD3 (Figure S4B) suggesting that in the tumor mass 15C4 results in inhibition of the SMAD2/3 arm of canonical TGFβ signaling.

The gene expression profiles of key endothelial cell adhesion molecules were also investigated as these have been reported to be suppressed in tumor vasculature and contribute to endothelial cell anergy. We observed elevated expression of most of the common adhesion molecules, with *Icam1* and *Vcam1* being significantly increased (Figure S4C), further supporting the contention that the vasculature is normalized by *Lrg1* deletion.

Inhibition of LRG1 increases the delivery and efficacy of chemotherapy

Whilst LRG1 may affect various aspects of tumor biology, we focused on the possibility that vascular normalization, through inhibition of LRG1, may be exploited to enhance the delivery of additional therapeutic agents. To test whether LRG1 blockade enhances the efficacy of a co-therapy, we first investigated 15C4 in combination with the cytotoxic agent cisplatin in the B16-F0 subcutaneous model. While both 15C4 and the maximum tolerated regimen of cisplatin each elicited a reduction in tumor size, their delivery in combination was significantly more effective (Figure 5A and Figure S5A). Analysis of the growth rates of individual tumors showed that the combined therapy of 15C4 and cisplatin was 25% more effective at inhibiting tumor growth than control IgG and cisplatin (Figure 5B). Consistent with this and the hypothesis that 15C4 enhances the delivery of cisplatin to the tumor, we saw a large increase in DNA double-stranded breaks, as revealed by γ-H2AX positivity (Figure 5C), and apoptosis (Figure 5D), demonstrating that inhibition of LRG1 improves the delivery, and hence efficacy, of a cytotoxic drug.

LRG1 inhibition enhances the efficacy of adoptive cell therapy

These results led us to ask whether a similar enhancement of tumor cell killing could be achieved with other therapeutic modalities. In particular, we sought to establish whether in such a generally treatment-refractory tumor we could enhance the effect of immunotherapies. We therefore investigated the combination of LRG1 antibody blockade and adoptive T cell therapy. Following subcutaneous grafting of B16-F10 melanoma cells harboring the internal influenza nucleoprotein antigen NP68 (NP68-B16)[37], donor F5B6 CD8^{+} T cells expressing a TCR specific for the NP68 peptide were transferred to the tumor-bearing host mice. As previously described[48], F5B6 CD8^{+} T cells significantly reduced tumor growth (Figure 6A and Figure S5B). However, the combination of 15C4 with this dose of adoptive T cells led to a 30% greater reduction in tumor growth rate (Figure 6A,B). Upon histological analysis the number of CD3^{+} T cells that had infiltrated the tumor increased

12

marginally in the 15C4 alone and donor CD8^{+} T cells groups but following combination therapy were elevated significantly, predominantly as a result of donor CD8^{+} T cell (CD90.2^{+}) infiltration (Figure 6C). The effects on tumor growth and T cell entry were replicated in a subsequent study in which the mice were treated with a reduced titer of F5B6 CD8^{+} T cells, but with the same dose of 15C4 antibody and extended for a further 13 days (Figure 6D and Figure S6A). Again, an increase in tumor infiltrating lymphocytes (TILs), particularly antigen-activated donor cells, was observed which is consistent with vascular normalization and improved delivery. We also observed less peritumoral T cell cuffing and an associated increase in the density of intratumoral TILs (Figure S6B), suggesting that migration from the tumor vascular margin through the stroma is also enhanced in 15C4 treated tumors.

LRG1 inhibition augments the effect of PD1 checkpoint inhibition

The use of immune checkpoint antagonists, including inhibitors of CTLA-4, PD1 and PD-L1, has proven to be very effective in the treatment of hematological cancers and melanoma but their impact on many solid cancers has been less effective. Having shown that 15C4 treatment enhanced the efficacy of adoptive T cell therapy we therefore investigated whether 15C4 could also augment the effectiveness of a checkpoint inhibitor. B16-F0 cells were grafted into wild type mice followed by treatment with 15C4, an anti-PD1 blocking antibody or a combination of both. As monotherapies, 15C4 and anti-PD1 each elicited a significant reduction in tumor volume (Figure 7A. Figure S6C) and mean growth rate (Figure 7B) with anti-PD1 producing 33% tumor growth inhibition (TGI). In combination with 15C4, however, overall TGI was 88% with evidence of tumor regression occurring at the later time point (Figure S6C). Histological analysis at study end point revealed increased CD8^{+} T cell infiltration in the combination therapy group (Figure 7C,D). Consistent with this, we also observed enhanced granzyme B expression (Figure 7C,E), indicative of greater cytotoxic lymphocyte activity.

To establish whether we could replicate this effect in another tumor model, we returned to the LLC subcutaneous tumor, which has been reported to be non-responsive to checkpoint inhibition[49-51]. Using an identical treatment strategy to that employed with the B16-F0 tumors, monotherapy with anti-PD1 did not impact on tumor growth whereas 15C4 treatment, as reported above, brought about a modest but significant reduction. Combination therapy, however, resulted in a significant reduction in tumor growth compared to IgG control ($P<0.0001$), or anti-PD1 ($P<0.002$) alone (Figure 7A). Moreover, as observed in the B16-F0 tumors we also recorded a change in the profile of infiltrated immune cells where a significant increase in $CD3^+$ T cells was observed (Figure S7B,C). Furthermore, the extent of granzyme B activity was also significantly increased in the combination arm (Figure S7D).

Combination of anti-LRG1 and anti-PD1 does not induce the formation of HEV

It has previously been shown that the combination of vascular normalizing agents and checkpoint inhibitors can stimulate the formation of HEVs and that this may play a significant role in driving enhanced leukocyte recruitment and subsequent improved tumor cell killing[52]. To determine whether our combined therapy also induced HEV formation, we undertook qPCR analysis of a panel of HEV signature genes, namely glycosylation-dependent cell adhesion molecule 1 (*Glycam1*), and the chemokines *Ccl19*, *Ccl21* and *Cxcl13*[14]. No significant differences in the expression of these genes between control and treatment arms was observed (Figure S7E) indicating that HEV induction did not contribute to the therapeutic effect. This was further confirmed by immunohistological staining of tumor sections with the MECA79 antibody, that detects peripheral node addressin (PNAd), revealing a lack of signal in control and treatment groups (Figure S7F). Similarly, in the LLC tumor we were unable to detect MECA79 staining showing that in this model LRG1 blockade also does not drive HEV formation (Figure S7G). These data indicate, therefore, that while HEV formation in other settings may be a contributing factor to the observed increase in TILs and treatment efficacy, it is not the only mechanism through which a combination of vascular normalizing strategies with immune checkpoint inhibition can elicit a beneficial effect.

DISCUSSION

In this study we provide new insight into the cause of dysfunctional vessel growth in tumors and show that LRG1 is a significant angiopathic factor capable of disrupting the normal angiogenic process and contributing to the pro-oncogenic microenvironment of primary tumors. Under normal conditions the principal source of LRG1 is the liver where it may serve as an acute phase protein[53] involved in wound healing[54,55]. In many diseases, however, LRG1 is induced locally in tissue lesions by the vascular endothelia and, in the case of cancer, by surrounding tumor cells. Locally produced LRG1 is known to contribute to the formation of abnormal vessels in the eye and kidney[1,2], in part by disrupting homeostatic TGFβ signaling in a highly context-dependent manner. Here we have shown that LRG1 also impacts on the vasculature of tumors and that deletion of the *Lrg1* gene, or inhibition of LRG1 function with a blocking antibody, improves vessel structure and function. Our data indicate that LRG1 is not directly pro-angiogenic but most likely facilitates neovascularization through its destabilizing effect on pericyte-endothelial cell interactions, a prerequisite for angiogenic sprouting[56]. The decrease in vessel density observed in some models, in the absence of *Lrg1* or following antibody blockade, may therefore reflect vascular stabilization and subsequent suppression of angiogenesis. These improvements in vessel function were mediated independently of any alterations in gene expression of cardinal ligand-receptor pathways involved in determining vascular status, including members of the VEGF signaling network. One gene that was found to be altered significantly was the shear response factor *Klf2*. Up-regulation of *Klf2* is consistent with a shift from turbulent oscillatory flow to uniform laminar flow and is in accordance with the observed vascular normalization[57]. KLF2 can be transcriptionally activated through TGFβ/ALK5 signaling[58] and is consistent with LRG1 biasing the TGFβ signaling in endothelium in favor of the destabilizing ALK1-Smad 1/5/8 pathway[1,2] and away from angiostatic ALK5-Smad2/3 signaling. *Lrg1* deletion, therefore,

15

may lead to maintenance of TGFβ/ALK5 signaling and vascular quiescence. Contrary to this, our observation that 15C4 causes a decrease in Smad3 phosphorylation in the tumor mass suggests that it affects TGFβ signaling differently in different cells within this setting, further illustrating the highly context dependent nature of the TGFβ signaling pathway. It has been reported that TGFβ1 enhances antigen-induced PD1 expression through Smad 3-dependent transcriptional activation in T cells[59] and that NK cell differentiation and anti-tumor function rely on Smad3 phosphorylation[60]. Its inhibition by a LRG1 blocking antibody may, therefore, contribute to an enhanced immune response and illustrates the growing evidence that LRG1 not only affects the vasculature but is also pleiotropic in its mode of action. Our observation that the *Notch2* gene is downregulated in tumor endothelial cells following 15C4 treatment points to LRG1 playing a role in the Notch pathway where it has a recognized role in promoting angiogenesis. Consistent with our finding of suppressed ERK phosphorylation, it has been shown that MAPK activation in cancer cells results in induction of Jagged1 and activation of angiogenesis though Notch signaling[61]. Clearly, these possibilities would require further investigation to establish a causal link.

The decrease in tumor growth and improvement in survival with deletion or blockade of LRG1 on its own may be a consequence of decreased angiogenesis, and/or due to associated effects on the tumor microenvironment. For example, improved oxygenation resulting from better perfusion is likely to reverse hypoxia-mediated changes such as activation of pro-oncogenic HIF1 mediated genes, selection and expansion of aggressive clones and immune evasion[62-65]. A further contributing factor may be a direct effect of LRG1 on cancer cells, where it has been reported to stimulate their proliferation and migration[34,66]. These deleterious effects of LRG1 are, however, at odds with a previous report of its suppression of LLC tumor growth[67], but are consistent with overwhelming clinical evidence that increased circulating LRG1 levels are diagnostic and associated with poor prognosis[27-39]. Our finding that blocking LRG1 in a metastatic model is of considerable potential

16

therapeutic importance, particularly as metastatic spread is the primary cause of cancer mortality. In a complementary study we have found that LRG1 primes the vasculature for metastatic seeding and that its inhibition renders metastatic sites less permissive for metastatic growth[68]. Moreover, it has also been reported recently that *Lrg1* knockout reduces B16F10 seeding to the lungs following intravascular tumor cell delivery[69] further corroborating LRG1 as a therapeutic target for reducing metastatic spread.

The discovery that LRG1 is angiopathic led us to test the hypothesis that blocking LRG1 would improve vascular function and augment the effects of other therapies. Treatment of tumor-bearing mice with 15C4 significantly enhanced the cytotoxic effect of cisplatin, suggesting that vascular normalization permits more effective delivery of the drug to the tumor mass. Indeed, combination of 15C4 and cisplatin exhibited not only reduced growth rate but also evidence of tumor regression that was not evident with monotherapy. The increased tumor cell death may also be enhanced through improved tumor oxygenation as hypoxia attenuates the effectiveness of cisplatin and contributes to chemotherapeutic resistance[70]. Consistent with the cisplatin study, blockade of LRG1 also improved the efficacy of adoptive T cell therapy. The B16-F0 mouse tumor model is not considered a very immunologically active tumor and, under normal conditions, exhibits limited TILs compared to other models. This was confirmed in B16-F10 melanoma cells expressing the NP68 internal influenza nucleoprotein antigen as a surrogate tumor antigen, where very few infiltrated CD3+ T cells were seen in the untreated mice. Adoptive cell therapy with NP68 antigen-specific CD8+ T cells led to reduced tumor growth but this did not correlate with a significant increase in the number of infiltrated CD3+ T cells in end-stage tumors, as has been noted previously in this model[71]. This is likely to reflect the dynamic nature of T cell involvement where single end-point analysis does not record possible temporal changes in T-cell recruitment, retention, exit, proliferation and death. Nevertheless, what was strikingly clear was that in the presence of LRG1 inhibition, adoptive T cell therapy led to greater tumor destruction and a significant increase in total CD3+ T cells that were predominantly

derived from the injected cells. This undoubtedly reflects the antigen activated status of the donor cells and their enhanced migratory and retention capacity compared to circulating naïve T cells. The improved vascular patency brought about by blocking LRG1 therefore results in better access to the tumor vascular bed enabling greater penetration into the tumor mass[72-74]. It is also likely that improved oxygenation will counteract some of the negative effects of hypoxia that may impact on T cell proliferation, retention and survival within the tumor microenvironment.

As with cisplatin and adoptive T cell therapy, blocking LRG1 with 15C4 also vastly improves the efficacy of a checkpoint inhibitor even in the highly resistant LLC model[49-51]. It has long been recognized that tumors can evade immune rejection through eliciting powerful immunosuppressive signals that prevent an effective T cell response. This negative immune regulation can be impeded through the use of immune checkpoint inhibitors[75,76], which in certain human cancers has led to marked improvements in tumor destruction and overall survival. However, many cancers remain immunologically silent for multifactorial reasons[77], but may include impaired immune cell delivery due to compromised perfusion[73,74]. This has led to the concept that vascular normalization strategies targeting VEGF, or other vascular modulating factors such as angiopoietin 2, endothelial glycoprotein L1, notch 1 and regulator of G protein signaling 5 (Rgs5)[22], may enhance effector cell entry to the tumor. These studies revealed is a profound crosstalk between the vasculature and the tumor immune microenvironment. Accordingly, vascular normalization promotes the infiltration of immune cells but can also enhance the expression of immune modulators such as the checkpoint ligand PD-L1[14-16]. Consistent with this crosstalk it has been reported that abnormalization of the vasculature decreases immune cell infiltration and that deletion of CD4^{+} T cells promotes dysfunctional vessels[25], revealing the close functional interplay between the immune system and the vasculature.

Improved lymphocyte infiltration previously reported with vascular normalization has been attributed to the formation of HEV[52]. These structures, normally present in lymph nodes, are characterized by a plump morphology and expression of specialized adhesion molecules, including peripheral node addressin (PNAd), that facilitate leukocyte traffic. Their induction in tumors, therefore, has provided a mechanistic explanation for the increased presence of TILs and enhanced tumor killing observed in combination therapies. In our setting, however, we were unable to observe the presence of HEV as determined by a panel of distinguishing markers. Other factors, over and above improved perfusion, may therefore be responsible for the enhanced infiltration observed. One feature of tumor endothelial cells that may contribute to poor leukocyte recruitment is their failure to respond effectively to activation by inflammatory mediators, a condition termed endothelial cell anergy[78]. This manifests in part as loss of expression of key cell adhesion molecules, such as ICAM-1 and VCAM-1[79,80], which are required for effective leukocyte recruitment[81]. Here we show that vascular normalization, brought about by *Lrg1* deletion, reverses in part this anergy through enhancing the induction of *Icam1* and *Vcam1* which in turn will facilitate the recruitment of circulating leukocytes[82]. This demonstrates that in addition to HEV formation, other mechanisms brought about by vascular normalization are at play in facilitating leukocyte tumor infiltration.

Our finding that inhibiting LRG1 with a function-blocking antibody reverses its detrimental effects on the tumor vasculature and enhances both adoptive T cell and immune checkpoint inhibition strategies lends further weight to the view that improving vascular function is a promising co-therapeutic strategy. Targeting LRG1, therefore, may provide an additional, or alternative, approach for normalizing the tumor vasculature and enhancing the efficacy of co-therapies. At present the principle approach is to employ anti-VEGF axis inhibitors which have shown some capacity to normalize the vasculature and improve immunotherapies[14]. However, major challenges with this approach remain not least of which is the difficulty in determining the appropriate dose and the purported short therapeutic window[6,9]. This is

confounded by difficulties in determining the relative activity of the VEGF axis in different tumors[13]. Unlike VEGF targeted therapies, blocking LRG1 has the potential advantage that patients may be stratified as higher circulating levels generally correlate with a worse prognosis[27-39].

As interest in vascular normalization increases various targets, other than those of the VEGF axis, have been identified[22] but for most their clinical utility remains untested. Here we present LRG1 as a promising target but its safety and successful translation into patients need to be proven. Unlike some targets, however, *Lrg1* knockout in the mouse does not produce an overt phenotype and they remain fertile and healthy over a normal lifespan providing evidence that it is not critical to homeostasis. In addition, as an ectopic non-essential modifier of TGFβ signaling, LRG1 blockade may offer advantages over direct therapeutic targeting of the TGFβ superfamily for treating cancer, which in general has been disappointing. Failure in this area is likely due to the difficulty in separating homeostatic from pathogenic TGFβ signaling as many core TGFβ signaling components are involved in both. TGFβ operates as an analogue signaling network whose effects are largely determined by a balance of complex, and nuanced, interactions between different arms of the extensive signaling cascade. Under normal conditions homeostatic TGFβ signaling is required for a stable vasculature but during disease this is disturbed and LRG1 is a prime disrupting candidate. However, targeting the LRG1 binding partner endoglin (ENG), which is upregulated on neovascular endothelia, has proven to be disappointing in achieving a therapeutic effect on tumor angiogenesis, although any impact on vascular normalization has not been fully investigated. This failure may be due, in part, to antagonizing a binding site important for maintaining vascular quiescence[83]. Interestingly, LRG1 binding to ENG facilitates the reconfiguration of the TFGβ receptor complex to enhance pathogenic signaling but in so doing may also result in loss of beneficial homeostatic BMP9/ENG signaling. Targeting LRG1, therefore, removes an independent pathogenic factor that disturbs the

homeostatic balance in TGFβ signaling without interfering with essential components of the network.

In conclusion, we have shown that LRG1 is a major driver of abnormal vessel growth in solid primary tumors and that its inhibition leads to significant restoration of normal vascular function. This raises the possibility that therapeutic targeting of LRG1 will improve the quality of vessels not only in cancer, but in diseases as diverse as diabetic kidney disease, neovascular age-related macular degeneration, and inflammatory disease, and pave the way towards improved strategies to revascularize ischemic tissue.

Limitations of Study

Whilst there is growing evidence that LRG1 is playing a role in human cancer, and the experimental animal work indicates its utility as a therapeutic target, the translatability of this approach to humans remains unproven. Work using subcutaneous tumor models in combination therapy will ideally need further corroboration in models that are considered more representative of human cancer. In particular, patient-derived xenograph models may provide additional evidence of efficacy although such models are complex and challenging when investigating the effect of immunotherapies. Nevertheless, despite these limitations the finding that LRG1 plays a role in genetically engineered mouse models and in a metastasis model provides confidence that this may be successfully translated into patients.

ACKNOWLEDGEMENTS

AUTHOR CONTRIBUTIONS

J.G. and S.E.M. conceived, designed and directed the overall study and had unrestricted access to all the data. A.A. and H.A.W. designed the adoptive T cell experiments and O.J.S. and R.J. the genetically engineered mouse model experiments. X.W. undertook the initial B16-F0 experiment. M.N.O., D.M.K., C.C., C.P., C.E.B. and J.W.D.B. performed all subsequent experimental work using the B16-F0 and LLC models. R.J., O.J.S. and M.N.O. conducted and analysed the experimental work using the genetic cancer models. M.N.O., D.M.K., C.P., C.C. L.D. and C.E.B. undertook the histological staining and analysis using the B16F0 and LLC model. M.N.O. and C.C. carried out the RNAScope *in situ* hybridization analysis. H.A.W., M.A. and J.O. conducted the adoptive T cell experiments. M.N.O., D.M.K., C.C. and C.P. performed the analysis of immune cell infiltration into tumours. L.D. and A.D. undertook the gene analysis studies. C.E.B. and J.W.D.B. carried out the human LRG1 ELISA analysis. M.S. and H.G.A. designed and undertook the mouse metastasis work. M.N.O. oversaw all the statistical analysis. J.Ge. and J.W.D.B. generated and purified the 15C4 blocking antibody. J.G. and S.E.M prepared the first draft of the manuscript, reviewed it and edited it with input from M.N.O., D.M.K., C.C. and collaborators A.A., R.J., O.J.S., M.S. and H.G.A., All authors contributed and agree to submission of the manuscript. All authors have read and approved the final draft and take full responsibility of its content, including the accuracy of the data and its statistical analysis.

DECLARATION OF INTERESTS

J.G. and S.E.M. are founders of a company spun out by UCL Business to commercialize a LRG1 function-blocking therapeutic antibody developed through the UK Medical Research Council DPFS funding scheme. This is currently directed towards treating ocular disease. J.G. and S.E.M. are members of the scientific advisory board and are shareholders of this company and named inventors on three patents related to LRG1 as a therapeutic target.

Figure 1. LRG1 is expressed in cancer. LRG1 protein expression (brown) in human cancers (A-C top images) and either normal tissue (A and C) or normal-appearing adjacent tissue (B) (bottom images). (**A**) lung squamous cell carcinoma, (**B**) prostate adenocarcinoma and (**C**), invasive ductal breast carcinoma. Scale bar A, B and C 200 μm. (**D**) Higher power images of increased LRG1 expression in vessel (arrow) from peritumoral breast carcinoma (left) compared with normal breast tissue (right). Scale bar, 60 μm. (**E**) Box and whisker plot showing serum LRG1 is increased, relative to healthy controls, in treatment naïve patients with colorectal adenocarcinoma (CRC), non-small cell lung carcinoma (NSCLC – squamous cell carcinoma) and pancreatic adenocarcinoma (n=15 per group). Kruskal-Wallis with Dunn post-test. Boxes extend from the 25th to 75th percentile. Whiskers represent the minimum and maximum datapoints. *P<0.05, **P<0.01, ****P<0.0001. *Lrg1* transcript expression in (**F**) B16-F0 and LLC syngeneic subcutaneous mouse tumors, (**G**) small intestine (left image intestine roll) of genetically engineered mouse cancer models *Apc^{Min/+}* and *vil^{CreER} Apc^{fl/+}* and (**H**) normal or diseased pancreas showing acinar ductal carcinoma (ADM), pancreatic intraepithelial neoplasia (PanIN) or PDAC from KPC mice. Scale bar 50μm. (**I**) Vascular *Lrg1* transcript expression (green) and immunohistochemical cell markers for endothelium (CD31; blue) and mural cells (αSMA; red) in mouse primary tumors. Scale bar, 30 μm. (**J**) Histological section through LLC lung metastasis and adjacent section labelled for *Lrg1* transcript (green) and endothelial cell markers ERG (red) and podocalyxin (white). Enlarged area shows tumor vessels expressing *Lrg1* transcript. Low magnification scale bar, 250 μm. High magnification scale bar, 50 μm.

Figure 2. *Lrg1* deletion reduces tumor volume and enhances survival. Growth curves of (**A**) B16-F0 and (**B**) LLC subcutaneous tumors in *Lrg1^{+/+}* and *Lrg1^{-/-}* mice (mean ± 95% CI). Repeated measure two-way ANOVA. (**C**) Kaplan-Meier survival curve of *Apc^{Min/+}* and (**D**) *vil^{CreER} Apc^{fl/+}* mice with or without homozygous deletion of *Lrg1*. Mantel-Cox test. (**E**) Tumor number in *Apc^{Min/+}* (*n*=16 *Lrg1^{+/+}* and *n*=27 *Lrg1^{-/-}*) and (**F**) *vil^{CreER} Apc^{fl/+}* (*n*=11 *Lrg1^{+/+}* and *n*=11 *Lrg1^{-/-}*) mouse small intestine (SI) and colon with or without homozygous deletion of

Lrg1. (**G**) Kaplan-Meier survival curve of KPC mice with or without homozygous deletion of *Lrg1*. Mantel-Cox test.

Figure 3. *Lrg1* deletion impacts on vascular structure. Vessel area (**A**) for different tumors expressed as the percentage of field that was positive for the endothelial cell marker CD31. (**B**) Representative images (from n>3) of CD31 stained sections of the vasculature from B16-F0, LLC and KPC tumors from $Lrg1^{+/+}$ and $Lrg1^{-/-}$ mice (scale bar, 50 μm) and (**C**) quantification of vessel density and size (cross-sectional area) of individual $CD31^+$ vessels. B16-F0 tumors (n=15 $Lrg1^{+/+}$ and n=17 $Lrg1^{-/-}$), LLC tumors (n=28 $Lrg1^{+/+}$ and n=25 $Lrg1^{-/-}$), KPC tumors (n=7 $Lrg1^{+/+}$ and n=10 $Lrg1^{-/-}$). 95% CI; Mann Whitney, with no corrections for multiple testing. (**D**) Mural cell (NG2 or αSMA) association with tumor endothelial cell (CD31 or podocalyxin) in B16-F0 and LLC tumors from mice with or without homozygous deletion of *Lrg1*. Tight association of $NG2^+$ mural cells with the tumor vessel is indicated by arrowheads. (**E**) Mural cell (αSMA) association with tumor endothelial cell (CD31) from KPC, $Apc^{Min/+}$ and $vil^{CreER} Apc^{fl/+}$ tumor models in wild type and *Lrg1* null mice. Tight association of $αSMA^+$ mural cells with the tumor vessel is indicated by arrowheads. For NG2, B16-F0 (n=10 $Lrg1^{+/+}$ and n=15 $Lrg1^{-/-}$ mice) and LLC (n=14 $Lrg1^{+/+}$ and n=15 $Lrg1^{-/-}$ mice). For αSMA, B16-F0 (n=11 $Lrg1^{+/+}$ and n=15 $Lrg1^{-/-}$ mice), LLC (n=7 $Lrg1^{+/+}$ and n=7 $Lrg1^{-/-}$ mice), KPC (n=5 $Lrg1^{+/+}$ and n=10 $Lrg1^{-/-}$ mice) and $Apc^{Min/+}$ (mean values from n=8 $Lrg1^{+/+}$ and n=11 $Lrg1^{-/-}$ mice). Scale bars, 100 μm. Student t-test. (**F**) Endothelial basement membrane (perlecan and/or collagen IV) association with tumor endothelium (CD31). For perlecan, B16-F0 (n=12 $Lrg1^{+/+}$ and n=11 $Lrg1^{-/-}$ mice) and LLC (n=19 $Lrg1^{+/+}$ and n=18 $Lrg1^{-/-}$ mice). For collagen IV, B16-F0 (n=12 $Lrg1^{+/+}$ and n=11 $Lrg1^{-/-}$ mice), LLC (n=19 $Lrg1^{+/+}$ and n=18 $Lrg1^{-/-}$ mice), KPC (n=4 $Lrg1^{+/+}$ and n=8 $Lrg1^{-/-}$ mice) and $Apc^{Min/+}$ (mean per mouse, n=5 $Lrg1^{+/+}$ and n=10 $Lrg1^{-/-}$ mice); Mann Whitney, *P<0.05, **P<0.01. Mann Whitney. (**G**) Scanning electron microscopy of blood vessels in B16-F0 tumors grown in $Lrg1^{+/+}$ or $Lrg1^{-/-}$ mice. Scale bar, 5 μm.

Figure 4. Antibody inhibition of LRG1 inhibits primary B16-F0 tumor growth, enhances survival in metastatic cancer and normalizes tumor vasculature. (**A**) Mean tumor volumes of B16-F0 tumors from wild-type mice treated with anti-LRG1 (15C4) or control antibody (IgG) (mean ± 95% CI). IgG, n=35 mice; 15C4, n=39 mice. RM two-way ANOVA. (**B**) Kaplan-Meier graph showing overall survival of mice after primary subcutaneous LLC tumor resection when treated with control IgG or 15C4 in perioperative setting (n = 10 mice per group; 50 mg/kg twice per week). Mice with primary tumor regrowth were excluded from the analysis. Mantel-Cox test. (**C**) Immunohistochemistry and quantification of mural cell (NG2 and αSMA) association with B16-F0 tumor endothelium (CD31 or podocalyxin) from wild-type mice treated with anti-LRG1 (15C4) or control antibody (IgG). Scale bar, 100 µm. 3D renders of the highlighted areas are shown. Graph shows fold change (mean ± S.E.M.) in mural cell overlap. For NG2, IgG n=11, 15C4 n=12. For αSMA, IgG n=16, 15C4 n=19 tumors. Student t-test. *P<0.05. Immunohistochemistry and quantification of (**D**) tumor vessel perfusion (lectin; n=12 tumors per condition; scale bar, 200 µm), (**E**) hypoxia (EF5; IgG, n=7; 15C4, n=5 tumors; scale bar, 1 mm), (**F**) adherens junction molecule (VE-cadherin; n=5 tumors per condition; scale bar, 50 µm), (**G**) permeability (Hoechst; IgG, n=11; 15C4, n=10 tumors; scale bar, 200 µm) and (**H**) tumor infiltrated lymphocyte density (CD3^{+} lymphocytes; IgG, n=13; 15C4, n=11 tumors; scale bar, 250 µm). For all graphs mean ± S.E.M.. Student t-test. *P<0.05, **P<0.01.

Figure 5. Antibody inhibition of LRG1 enhances the efficacy of cisplatin. Treatment of B16-F0 tumors with 15C4 (50 mg/kg) and cisplatin (2.5 mg/kg). (**A**) Growth curves (mean ± S.E.M.), analyzed by linear regression comparing to No IgG (*P<0.05, ****P<0.0001) or pairs as shown ([####]P<0.0001). No IgG, n= 13; IgG, n=28; 15C4, n=33; IgG + Cisplatin, n=23 and 15C4 + cisplatin, n=27 mice. (**B**) Growth rate (slope) of each tumor. Student t test, *P<0.05, **P<0.01. (**C**) DNA double strand breaks detected with antibody against γ-H2AX (green).

DAPI shown in blue. Scale bar, 30µm. Graph shows percentage of γ-H2AX$^+$ nuclei (mean ± 95% CI). One-way ANOVA, **$P<0.01$. IgG, $n=6$; 15C4, $n=9$; IgG + cisplatin, $n=15$ and 15C4 + cisplatin, $n=17$ mice. (**D**) Apoptotic cells revealed by TUNEL staining (green). DAPI shown in blue. Scale bar, 30µm. Graph shows density of TUNEL$^+$ apoptotic cells (mean ± S.E.M.). Student t test, **$P<0.01$. IgG + Cisplatin, $n=22$ and 15C4 + cisplatin, $n=22$ mice.

Figure 6. Antibody inhibition of LRG1 improves the efficacy of adoptive T cell therapy.
Treatment of mice bearing NP68-expressing B16-F10 subcutaneous tumors with 15C4 and F5B6 cytotoxic T-cells. (**A**) Growth curves (mean ± S.E.M.), analyzed by linear regression comparing to No Transfer (****$P<0.0001$) or pairs as shown ($^{###}P<0.001$, $^{####}P<0.0001$). No Transfer, $n= 9$; IgG, $n=10$; 15C4, $n=11$; IgG + F5B6, $n=10$ and 15C4 + F5B6, $n=11$ mice. (**B**) Growth rate (slope) of each tumor. Student t test, *$P<0.05$, **$P<0.01$, ***$P<0.001$. (**C**) T-cell infiltration of tumors taken from animals shown in A above. Scale bar, 200 µm. Graphs show density (objects/mm^2) of CD3$^+$ T cells (top) and of CD90.2$^+$ donor cells (bottom). Student t-test, *$P<0.05$, **$P<0.01$. (**D**) As in (**A**) but with reduced F5B6 cytotoxic T cell treatment. Graphs show density (objects/mm^2) of CD3$^+$ T cells (left) and of CD90.2$^+$ donor cells (right). No transfer, $n= 8$; IgG + F5B6, $n= 10$; 15C4 + F5B6, $n= 10$. Linear regression. *$P<0.05$, **$P<0.01$, ***$P<0.001$.

Figure 7. Inhibition of LRG1 with a blocking antibody improves the efficacy of checkpoint inhibition.
Treatment of B16-F0 subcutaneous tumors with 15C4 and anti-PD1. (**A**) Growth curves (mean ± S.E.M.), analyzed by linear regression comparing pairs as shown. (**B**) Growth rate (slope) of each tumor. Student t test. (**C**) CD8$^+$ (red) and granzyme B$^+$ (green) T-cell infiltration of tumors. SAPI shown in blue. Scale bars, 500 µm (top) and 150 µm (bottom). Graphs show density (objects/mm^2) of CD8$^+$ T-cells (**D**) and granzyme B area fraction (**E**). $n= 9$, 10, 6, 4 for **A** and $n=8$, 6, 6 and 8 for **D** and **E**, tumors. Student t-test, *$P<0.05$, ***$P<0.001$, ****$P<0.001$.

RESOURCE AVAILABILITY

Lead Contact

Further information and requests for resources and reagents should be directed to and will be fulfilled by the lead contact, John Greenwood (j.greenwood@ucl.ac.uk).

Materials availability

This study did not generate new unique reagents.

There are restrictions to the availability of the anti-LRG1 antibody 15C4 due to production limitations and the requirement for an MTA.

Data availability

Data presented in this manuscript is freely available.

The RNASeq datasets generated during this study are available at NCBI Sequence Read Archive https://www.ncbi.nlm.nih.gov/sra/PRJNA552723 and NCBI Gene Expression Omnibus https://www.ncbi.nlm.nih.gov/geo/query/acc.cgi?acc=GSE184816.

EXPERIMENTAL MODEL AND SUBJECT DETAILS

Human samples

Fresh frozen normal lung and lung squamous cell carcinoma tissue were obtained from Proteogenex Inc (https://www.proteogenex.com). Formalin-fixed paraffin-embedded prostate cancer tissue was obtained from Amsbio (https://www.amsbio.com) and normal human breast and ductal breast carcinoma from Pantomics Inc (https://www.pantomics.com). Human serum samples from normal healthy subjects and from treatment naïve cancer patients with colorectal adenocarcinoma, pancreatic adenocarcinoma and squamous cell lung carcinoma, were obtained from Proteogenex, Inc.

Mice

All procedures in the UK were performed in accordance with the UK Animals (Scientific Procedures) Act and the Animal Welfare and the Ethical Review Bodies of the UCL Institute

28

of Ophthalmology, Cancer Research UK Beatson Institute, University of Glasgow, and Cardiff University. All procedures in Germany were approved by governmental (G164/16, G231/16, G254/18, G286/18, G9/19, G196/19, and G213/18 from Regierungspr.sidium Karlsruhe, Germany) and Institutional (IRCBC-2018-006 to J.H.) Animal Care and Use Committees. All experiments were performed in accordance with the respective institutional guidelines for the care and use of laboratory animals. All mice were housed in specific pathogen–free animal facilities had a 12-hour light/12-hour dark cycle with free access to food and drinking water. Where possible, preliminary experiments were undertaken to establish sample sizes, whilst addressing ethical and reductionist animal use considerations. For subcutaneous graft models male C57BL/6J mice of 7-8 weeks of age were purchased from Harlan Laboratories or Charles River Laboratories. *Lrg1*^{−/−} mice were generated by the University of California Davies knockout mouse project (KOMP) repository (http://www.komp.org/) and bred in-house. Genetically engineered male and female mice were bred and housed in the animal facility at the CRUK Beatson Institute. All experiments on genetically engineered mouse models were performed on a C57BL/6 background. For the metastatic model C57BL/6N mice were purchased from Charles River Laboratories and used between 8 and 12 weeks of age. All mice were housed in the DKFZ animal facility on a 12-hour light/12-hour dark cycle with free access to food and drinking water in specific pathogen–free animal facilities.

METHOD DETAILS

Cell Culture

Mouse cancer cell lines B16-F0 (mouse melanoma cell line), NP68-B16 (mouse melanoma B16F10 cells expressing NP68 peptide and LLC1 (LL/2; mouse Lewis Lung carcinoma) were maintained in Dulbecco's Modified Eagle's Medium supplemented with glucose (4.5 g/L), sodium pyruvate (110 mg/L), 10% FBS, penicillin (100,000 U/L) and streptomycin sulphate (100 mg/L) at 37°C in 5% CO_2 and checked to be clear of mycoplasma contamination.

Tumour models

For subcutaneous tumors single-cell suspensions of 1×10^6 B16-F0 or LLC cells were injected subcutaneously into a single dorsal flank of $Lrg1^{+/+}$ or $Lrg1^{-/-}$ 8-16 week old male C57BL/6J mice in 100 µl PBS. Mice were randomized by age prior to inoculation. Tumors were measured by evaluators, blinded to treatment, at defined intervals using calipers and tumor volume was calculated using the formula: $V = (4/3) \times \pi \times (L/2) \times (W/2) \times (H/2)$. Mice were sacrificed at the end of the experiment, or when tumors reached the permitted humane endpoint. The mean tumor growth rate for individual tumors was calculated using the slope of log transformed tumor volumes[71].

For ageing experiments in the $Apc^{Min/+}$ and KPC genetically engineered spontaneous mouse tumor models[84,85], mice were sampled when showing moderate signs of illness. Tumors in $villin^{CreER} Apc^{fl/+}$ mice[86,87] were induced at an age of 6-10 weeks by a single intra peritoneal injection of 2 mg Tamoxifen in corn oil, and aged until showing moderate signs of illness. No distinction between males and females was made in any of the mouse experiments and researchers were blinded for $Lrg1$ status.

In the metastatic model LLC tumors were allowed to develop following subcutaneous inoculation of 1×10^6 LLC cells in PBS in C57BL/6N mice. Primary tumours were surgically resected at an average size of 300 mm^3. Perioperative treatment was initiated once the primary tumour size reached an average of 150 mm^3 and continued until 10 days following primary tumour resection. Tumors were resected at an average size of 300 mm^3. Mice were administered with either anti-LRG1 (15C4) or control IgG (50 mg/kg) twice a week and routinely checked for the experimental endpoint criteria. Mice were randomly assigned by a blinded scientist into the cohorts of treatment at the time of therapy initiation. For the RNAscope analysis of metastases-bearing lung tissue, samples were collected approximately three weeks post-primary tumor resection.

ELISA

96 well Maxi-Sorp immunoplates (Fisher 10547781) were coated with 40 µg/ml 15C4 (50µl/well) in 0.2M $NaCO_3/NaHCO_3$ buffer pH9.4 and incubated overnight at 4°C. The plates were washed 3 times with 0.1%Tween-20/PBS, blocked with 3% BSA/PBS for 1h at RT and washed again 3 times. Patient samples and LRG1 standards (range 0 - 6000ng/ml) were diluted with 0.1%Tween-20/PBS and left to incubate overnight at 4°C. Plates were washed 3 times before adding anti-LRG1 pAb (Atlas Antibodies) in PBS and incubated for 1.5h at room temperature. Plates were washed 3 times before adding HRP goat anti-rabbit (Dako) in PBS for 1.5h at room temperature. The plates were washed 3 times and ELISA substrate reagent kit (R&D Systems) was used at 1:1 ratio and left to develop in the dark. 2N sulphuric acid was used to stop the reaction and plates were read at 450nm (reference wavelength 540nm).

Immunohistochemistry

Human tumor sections: For human lung tissue, cryosections were cut at a nominal 5µm thickness, washed, blocked with milk powder and stained with humanized 15C4 (Magacizumab) or natural human IgG4 (Abcam) that were FITC conjugated using the commercial FluoroTag conjugation kit (Sigma-Aldrich). Following washing and blocking with milk powder, primary antibodies were incubated for 1h at room temperature at a concentration of 0.078µg/ml. Sections were washed and treated with Dako Envision[+] system HRP labeled polymer anti-rabbit for 30min. After further washing sections were treated with Liquid DAB+ substrate chromogen system for 10min and 0.5% copper sulphate solution for 5min followed by counterstaining with haematoxylin for 1min.

Formalin-fixed paraffin-embedded sections of prostate or breast tissue were cut at 5µm thickness and treated with either anti-LRG1 rabbit polyclonal antibody (Proteintech) at 1:200 dilution or anti LRG1 monoclonal antibody 15C4 at 10µg/ml. Following antigen heat retrieval with a Leica ER2, sections were processed on the Leica Bond III platform.

Paraffin embedded mouse tumor sections: the small intestine and colon from $Apc^{Min/+}$ and the $vil^{CreER} Apc^{fl/+}$ tumors were formalin-fixed and paraffin-embedded (FFPE). 5 µm sections were deparaffinized and immunolabelled following antigen retrieval before being fixed in 4% paraformaldehyde, 100% methanol or 100% acetone, depending on antibodies used. Sections were blocked in 0.5% BSA and washed in 0.01% Tween-20 in PBS.

Fresh frozen mouse tumor sections: subcutaneous B16-F0, LLC, KPC and PDAC tumours were fresh frozen on dry-ice and embedded in optimal-cutting-temperature medium (OCT). Contiguous frozen tissue sections were cut at a thickness of 8 µm or 20 µm and stored at −20°C. Sections were fixed immediately in 4% paraformaldehyde, 100% methanol or 100% acetone, washed in PBS, permeabilized in 0.1% Tween-20 in PBS for 10min, washed again in PBS and blocked in 1% BSA for 1h at room temperature. Primary antibodies were incubated overnight at 4°C in 0.5% BSA with or without 0.01% Triton-X100 in PBS. The antibodies used to label mouse endothelium were anti-CD31 (Dianova or Abcam), endomucin (Abcam), anti-VE-cadherin (Santa Cruz) and anti-podocalyxin (PDXL; R&D systems), with the latter used in B16-F0 tumours as it strongly labelled the endothelium and the staining pattern was almost indistinguishable from CD31 in this model (data not shown). Mural cells were labeled with antibodies to NG2 (Merck-Millipore) or αSMA (Sigma-Aldrich). Antibodies to basement membrane proteins collagen-IV (Merck-Millipore) or perlecan (Abcam), and immune cell markers CD3 (Abcam), CD8 (Novus), or CD90.2 (Biolegend) were also used. Other primary antibodies were to granzymeB (Novus) and EF5 (Merck-Millipore). Alexa-fluor labeled secondary antibodies (Thermofisher) were incubated in 0.5% BSA with or without 0.01% Triton X100 at room temperature for 1h. Both primary and secondary antibodies were washed three times for 15 min, either in 0.01% Tween-20 in PBS or PBS only, depending on the antibody. The slides were mounted using anti-fade mounting medium (ProLong Gold or Dako). For the CD8 and granzymeB co-staining protocol, samples were processed as described above except that they were fixed in 2% PFA in PBS, dropped in PBS, fixed again for 3min in methanol at -20°C, washed in distilled water and 0.01%

Tween-20 in PBS for 5min. The antibodies (1:100) were incubated in 0.5% BSA with 0.001% Triton X100 in PBS.

RNAScope® *in situ* hybridisation

FFPE tumor or intestine samples were placed in xylene followed by absolute ethanol. For chromogenic detection, slides were processed using the 2.0 HD Detection kit – BROWN (Advanced Cell Diagnostics) and the manufacturer's instructions. For fluorescence detection, slides were processed using the Multiplex Fluorescent Kit v2, followed by TSA® signal amplification (PerkinElmer) and immunohistochemistry performed afterwards if desired. Slides were hybridized with probes specific to *Lrg1* and the quality of signal and tissue were determined using positive (*Ppib*) and negative (*Dapb*) probes, supplied by the manufacturer (Advanced Cell Diagnostics). The specificity of the *Lrg1* probe was confirmed by probing tumor sections from *Lrg1$^{+/+}$ and Lrg1$^{-/-}$* mice.

Analysis of vessel density and normalisation

To measure vessel profiles in the tumors, sections were labeled with antibodies to endothelium markers (CD31, podocalyxin (PDXL) or endomucin). B16F0 and LLC sections were imaged using a Nikon Eclipse Ti epifluorescence microscope (Nikon). The entire tumor vasculature was included in the analysis, excluding vasculature in the tumor margin. KPC sections were imaged on a Zeiss 700 confocal microscope. At least two 850x850 μm areas per section containing tumor vessels were imaged and maximum intensity projections of z-stacks analyzed. Vessel density (number per unit area) and size (cross-sectional area) were calculated from thresholded images from B16-F0, LLC and KPC tumors using NIS-Elements software (Nikon). Vessels were identified as individual objects between 5-800 μm^2 that were positive for the endothelial marker. The mean vessel size and density per tumor section is reported. For *Apc$^{Min/+}$* and the *vil^{CreER} Apc$^{fl/+}$* sections, at least 2 intestinal adenomas per mouse were imaged, using a Zeiss 700 confocal microscope and the mean result reported. Vessels in a 250x188 μm ROI at the luminal edge of the adenoma were analyzed. Since

vessels were mostly contiguous in these images, vessel area per image was calculated using ImageJ, rather than vessel size and density of individual vessels.

The association of mural cells or basement membrane proteins with the tumor endothelium was measured from sections labelled with antibodies to endothelial cells (CD31, endomucin or podocalyxin) and multiple mural cell (NG2 and/or αSMA) or matrix (perlecan and collagen IV) markers. For mural cells, a 0.37 or 0.72 cm^2 ROI encompassing the edge and core of the tumor was imaged and then analyzed using NIS elements software (Nikon) or ImageJ (http://imagej.nih.gov/ij/). For analysis of endothelial basement membrane, at least 2 640x640 µm areas per section containing tumor vessels were imaged on a Zeiss 710 microscope and maximum intensity projections of z-stacks analyzed. The fraction of perlecan or collagen IV pixels which overlap CD31 positive pixels was calculated from a single plane though the center of the z-stack. The same threshold was used for each image and Manders' overlap coefficient was calculated using JACoP plugin on ImageJ. Data were normalized to the mean control value for each experiment. In all cases images were anonymized with respect to experimental condition before analysis.

Tumor hypoxia and vascular perfusion

To measure tumor hypoxia, 0.2 ml of 10mM EF5 (Merck-Millipore) was injected into the peritoneum of tumor bearing mice and tumors harvested after 1h. Pimonidazole adducts in sections were detected by immunohistochemistry using anti-EF5, clone ELK3-51 Cyanine 3 conjugate and the entire tumor section imaged using a Nikon Eclipse Ti epifluorescence microscope. The proportion of each tumor positive for hypoxia stain was measured from identically thresholded images on NIS elements software (Nikon) and reported as a percentage of total image area.

To examine tumor vessel perfusion and leakage, tumor-bearing mice were injected intravenously with FITC-labelled Lycopersicon esculentum lectin (Vector labs; 10 mg/kg) and

low molecular weight fluorescent DNA binding dye Hoechst 33342 (Sigma-Aldrich; 7.5 mg/kg), respectively, followed 3min later by perfusion fixation with 4% paraformaldehyde. Cryosections were labelled with an antibody to endomucin to count endothelialized vessels. The percentage of perfused vessels was calculated as the % of endomucin+ vessels which were also lectin+. The proportion of each ROI positive for Hoechst was measured from thresholded images on NIS elements software (Nikon), and normalized to lectin area, i.e. perfused vessels.

Tumor co-therapy strategies

Chemotherapy: To investigate the effects of LRG1 blockade on efficacy of tumor chemotherapy, wild-type C57BL/6 mice were injected with B16-F0 cells subcutaneously into the dorsal flank and treated with 50 mg/kg of the function-blocking anti-Lrg1 monoclonal antibody 15C4 or IgG control administered by intraperitoneal injection every 3 days from day 3. At day 7 and every other day thereafter, a maximum tolerated dose (2.5 mg/kg) of the chemotherapy drug cisplatin was administered by intraperitoneal injection until the mice were sacrificed at the end of the experiment or when tumors exceeded 1000 mm³. Cisplatin-induced DNA damage was assayed using an antibody against the DNA double strand break marker gamma-H2AX (Merck-Millipore) on tumor sections co-stained with DAPI to enumerate cell nuclei. The percentage of nuclei with gamma-H2AX foci was measured from confocal images (Zeiss 700) and analyzed by evaluators who were blinded to the experimental arm. Apoptotic cells were identified by TUNEL assays on sections using an ApopTag in situ apoptosis detection kit (Merck-Millipore).

Adoptive T cell therapy: To investigate the effects of LRG1 blockade on the efficacy of tumor immunotherapy a mouse model of adoptive T cell therapy was used as described[48]. Briefly, 5x10⁵ NP68-B16 melanoma cells in 200µl sterile PBS were injected subcutaneously into the shaven left dorsal flank of B6.PL-Thy1a/CyJ (Thy1.1/CD90.1) or C57BL/6 (Thy1.2/CD90.2) mice, tumors were grown for 6 days and the mice sub-lethally irradiated with 597cGy total body irradiation. On day 7, F5B6 CD8+ T cells (> 95% naive (CD62L+, CD44 low) CD8+ T

cells) expressing the F5 T cell receptor for NP68 peptide on a C57BL/6 background were isolated from spleens of naïve F5B6 mice using a CD8α⁺ T cell isolation kit for negative selection, and LS columns, according to the manufacturer's instructions (StemCell Technologies). Briefly, spleens were harvested from adult mice and mashed through a 70 µm cell strainer (BD Pharmingen). Red blood cells were lysed using red cell lysis buffer (Biolegend) and lymphocytes washed with ice-cold phosphate buffered saline (PBS) supplemented with 2% fetal calf serum (FCS) prior to magnetic isolation. The enriched CD8⁺ cell fraction was counted using a hemocytometer, resuspended in sterile PBS for injection and analyzed for CD8, CD62L, CD44, CD27 and F5 TCR expression. Tumor-bearing mice were randomly distributed into 5 treatment groups of 8-11 mice (No transfer; IgG; 15C4: IgG + F5B6; 15C4 + F5B6) and injected subcutaneously with peptide vaccine (100µg NP68 peptide in 200µl incomplete Freund's adjuvant) into the right flank prior followed by 2.25×10^5 F5B6 CD8⁺ T cells (CD90.2) injected into the tail vein. Mice were treated with 50 mg/kg of the function-blocking anti-LRG1 mouse monoclonal antibody 15C4 or IgG control administered by intraperitoneal injection commencing on the same day as T cell transfers and antibody administration was repeated every 3 days until the end of the study. Tumors were measured with calipers as described above. At the end of the experiment, mice were sacrificed and tumors were frozen on dry-ice in optimal-cutting-temperature medium (OCT) and stored at −80°C before immunostaining for either total T cells (CD3⁺) or for donor T cells (CD90.2 in tumors grown in CD90.1 mice).

Immune checkpoint blockade: To investigate the effects of LRG1 blockade on the efficacy of PD1/PDL1 axis blockade in an immunologically resistant tumor, wild-type C57BL/6J male mice 8-10 weeks of age were injected with 1×10^6 B16-F0 cells subcutaneously into the flank. Mice were treated with a combination of 50 mg/kg of the function-blocking anti-LRG1 antibody 15C4, 200 µg rat anti-mouse PD1 (Bio X Cell) or 200 µg rat IgG2a isotype control (Bio X Cell). Mice were dosed by intraperitoneal injection commencing on day 3 and antibody administration was repeated every 3 days until the end of the study. Tumors were measured with calipers at defined intervals and tumor volumes were calculated. At the end

of the experiment, mice were sacrificed and tumors were fresh frozen on dry-ice in OCT and stored at −80°C before immunostaining.

T-cell infiltration analysis

Fresh-frozen sections were fixed in 100% ice-cold methanol and/or 4% formaldehyde and labeled using antibodies to total T cells (CD3$^+$), donor T-cells (CD90.2$^+$), cytotoxic T cells (CD8$^+$) and/or granzyme B. For each section a 2920x2920 μm or 4250x4250 μm tile scan was acquired encompassing the edge and core of the tumor, using a Zeiss 710 confocal microscope. Alternatively, whole sections were imaged using the EVOS Imaging System. Maximum intensity projections of z-stacks were analyzed using NIS elements software (Nikon). Positive cells were identified by thresholding either as objects/area or as fraction of total image area.

Scanning Electron Microscopy

14 days after subcutaneous B16F0 injection, *Lrg1$^{+/+}$* and *Lrg1$^{-/-}$* mice bearing tumors were perfusion-fixed with Karnovsky fixative (2% paraformaldehyde, 2.5% glutaraldehyde), followed by immersion fixation in fixative overnight at 4°C. Vibratome sections (200 μm) were washed in PBS and then osmicated with 1% osmium tetroxide in ddH$_2$O for 1h. They were then washed in ddH$_2$O and dehydrated in alcohol. The tumor sections were then immersed in dry methanol and in hexamethyldisilazane (reagent grade >99%, Aldrich chemicals) and allowed to dry. The specimens were fixed onto aluminum stubs using a conductive carbon disc and silver paint (Agar) and were then coated with 2 nm platinum in a Cressington sputter coater. Imaging was done on a Zeiss Sigma VP SEM using the in lens detector.

RNASeq and RT-qPCR

RNA from *Lrg1$^{+/+}$* and *Lrg1$^{-/-}$* B16F0 tumors was extracted using the RNeasy mini kit (Qiagen) and analyzed for quality using the 4200 TapeStation (Agilent). mRNA was

prepared from total RNA for sequencing using the Kapa riboerase library preparation kit (Agilent) and was sequenced for differential expression analysis (0.5 High output NextSeq run, 43bp paired end reads). Deseq2 method was used in R to identify differentially expressed transcripts Raw RNA sequence data have been deposited with NCBI Sequence Read Archive accession number PRJNA552723

(https://www.ncbi.nlm.nih.gov/sra/PRJNA552723).

Endothelial cells were isolated from the CD45-negative fraction of 15C4 or IgG control treated B16F0 tumors by cell sorting with a FITC-labelled anti-CD31 antibody. The FACS-sorted cell population was isolated in RLT RNA extraction buffer (Qiagen) and RNA quality was analysed using the 4200 TapeStation (Agilent). First strand cDNA synthesis was followed by PCR-amplification, and amplified cDNA was purified using beads and the cDNA libraries were made using the Nextera XT kit. Sequencing was performed on an Illumina NextSeq 500 with a 75bp single read and 8bp Unique Molecular Identifier. Sequencing reads were generated for each sample before aligning to the mouse genome. Differential expression and clustering were performed from the count data using the BioConductor packages SARTools and DESeq2. Processed count files and metadata have been deposited at NCBI Gene Expression Omnibus with accession number GSE184816

(https://www.ncbi.nlm.nih.gov/geo/query/acc.cgi?acc=GSE184816).

For RT-qPCR analysis, total RNA was isolated from B16-F0 tumors that were treated with 15C4 or irrelevant IgG as indicated in the experimental conditions. cDNA was synthesized using the LunaScript RT SuperMix Kit (New England Biolabs E3010) and gene expression was analyzed by RT-qPCR on QuantStudio 6 (Applied Biosciences) using the Luna Universal qPCR kit (New England Biolabs, M3003). Relative expression was normalized to *Actb* and *Gapdh* housekeeping genes and was determined using the ΔΔCt method. Primer sequences for the mouse genes were as follows: *Ccl19*, Forward: CAGTCACTCCCCTGTGAACC, Reverse: CAGAGTTGGGGCTGGGAAG, *Ccl21a*, Forward: AAGGCAGTGATGGAGGGGGT, Reverse: CTTAGAGTGCTTCCGGGGTG, *Cxcl13*, Forward: CAGGCCACGGTATTCTGGA, Reverse: CAGGGGGCGTAACTTGAATC,

Glycam1, Forward: TCAGCTGCAACCACCTCAG, Reverse:

TTCGTGATACGACTGGCACC.

Tissue lysate preparation and Western blotting

Frozen tumor samples (~10mg per sample) were lysed in 300 µl RIPA buffer supplemented

with protease and phosphatase inhibitors. The lysates were homogenized using a pestle and

mortar, followed by 30min incubation on ice with vortexing every 5min. The lysates were

then centrifuged at maximum speed (21,000 x g) for 20min at 4°C, and protein concentration

was estimated using a BCA colorimetric protein assay (Pierce). Lysates were subjected to

SDS-PAGE and Western blotting. Specific antibodies (Cell Signalling) against p-Akt, total-

Akt, p-Erk1/2, total-Erk1/2, p-Sapk/Jnk, total-Sapk/Jnk, p-p38, total-p38, p-Smad3 and total-

Smad2/3 were used. GAPDH served as a housekeeping gene. Densitometry analysis was

performed using ImageJ software.

QUANTIFICATION AND STATISTICAL ANALYSIS

All analyses were blinded. Statistical analysis was performed using Graphpad Prism version

5.0 or 7.0 for Windows (GraphPad Software, La Jolla California USA, www.graphpad.com).

Definition of centre, exact n, error bars and statistical tests used for each experiment are

indicated in the figure legends. All error bars show 95% confidence interval (CI) unless

otherwise stated. All t tests were two-tailed. Bonferonni corrections were applied for multiple

comparisons using ANOVA, unless otherwise stated. A *P* value less than 0.05 was

considered statistically significant. Grubb's test was used to test for outliers

(www.graphpad.com), which were removed before analysis. For in vivo studies, group sizes

were determined using historical data to reach a statistical power of at least 80% for the

relevant effect size (http://powerandsamplesize.com). For all figures p values are

represented as followed: *p < 0.05; **p < 0.01; ***p < 0.001, ****p < 0.0001

SUPPLEMENTAL FIGURE LEGENDS

Supplemental Figure 1. *Lrg1* **is minimally expressed in normal tissue but is highly expressed in the liver.** RNAScope® *in situ* hybridization of sections from wild-type (non-tumor bearing) mouse tissue showing skin, pancreas and normal intestine, do not express *Lrg1*. Positive control transcript *Ppib* (**A**) or *Lrg1* (**B**) signal and immunohistochemical staining of endothelial cells (CD31). Scale bar, 100 μm. (**C**) Schematic illustration of LLC spontaneous metastasis model, in which mice develop lung metastases following primary tumor resection. (**D**) RNAScope® *in situ* hybridization for *Lrg1* in sections of wild type mouse liver (positive control), *Lrg1⁻ᐟ⁻* mouse liver, and normal lung counterstained with antibodies against ERG and podocalyxin showing negative *Lrg1* expression in normal mouse lung. DAPI shown in blue. Region in hashed box enlarged on the right and split into separate channels. Scale bar, 50 μm.

Supplemental Figure 2. **Effect of** *Lrg1* **knockout or LRG1 inhibition on tumor growth and vascular structure.** Individual growth curves (from data shown in Figure 2A,B) for B16-F0 (**A**) and LLC (**B**) subcutaneous tumors from *Lrg1⁺ᐟ⁺* or *Lrg1⁻ᐟ⁻* mice. Immunohistochemical staining for tumor vascular density **(C)** and association with basement membrane **(D)** in colorectal cancer models**.** (**C**) CD31 stained sections of the vasculature from *Apc^{Min/+}* and *vil^{CreER} Apc^{fl/+}* adenomas from *Lrg1⁺ᐟ⁺* and *Lrg1⁻ᐟ⁻* mice. Scale bar, 50 μm. (**D**) Endothelial basement membrane association with tumor vessels in sections labelled with antibodies to CD31, perlecan and/or collagen IV. Scale bar, 100 μm. (**E**). Individual growth curves of data shown in Figure 4A of B16-F0 tumors from wild-type mice treated with control antibody (IgG) or anti-LRG1 (15C4) (mean ± 95% CI). IgG, *n*=35 mice; 15C4, *n*=39 mice. RM two-way ANOVA. (**F**). Vascularity of B16-F0 tumors from WT mice treated with control antibody (IgG) or anti-LRG1 (15C4) revealed by CD31 immunohistochemistry. Scale bar, 250 μm. Graphs show percentage of CD31⁺ area in the image, and vessel density and cross-sectional area of individual CD31⁺ objects (mean ± 95% CI). IgG, *n*=14 tumors; 15C4, *n*=18 tumors. Mann

Whitney test. *P<0.05, ****P<0.0001. (**G**) Endothelial basement membrane association with tumor vessels from wild-type mice treated with IgG or 15C4. Sections were labelled with antibodies to CD31, perlecan and/or collagen IV. Scale bar, 100 µm. Overlap with endothelium was measured and normalized to mean control value in each experiment (mean ± sem). IgG *n*=12, 15C4 *n*=13.

Supplemental Figure 3. **Expression of genes associated with vascular function.** Differential expression of key genes involved in vascular maturation or destabilization identified by RNASeq analysis. Genes are grouped into families and expressed as fold change in whole B16-F0 tumors in *Lrg1*$^{-/-}$ mice compared to tumors from *Lrg1*$^{+/+}$ mice. N=3 for each group. (**A**) or from B16-F0 tumor vessel endothelial cells isolated from wild type mice treated with anti-LRG1 antibody 15C4 compared to control IgG treated animals. N=3 for each group. (**B**). P-value adjusted for multiple testing using the Benjamini-Hochberg method. *P < 0.05.

Supplemental Figure 4. **Effect of LRG1 inhibition on TGFβ associated signaling pathways and adhesion molecules.** Western blot analysis for phosphorylated signaling components associated with non-canonical (**A**) and canonical (**B**) TGFβ signaling pathways. GAPDH was used as a sample integrity control. Bar graphs show the densitometric analysis of the ratio of phosphorylated to total proteins after normalization to GAPDH (N≥5 per group). Non-parametric unpaired t-test. *P<0.05, **P<0.01. (**C**) Gene expression of key endothelial cell adhesion molecules involved in leukocyte recruitment in B16-F0 tumors from *Lrg1*$^{-/-}$ mice compared to wild type controls. N=3 per group. RNASeq data expressed as fold change.

Supplemental Figure 5. B16-F0 tumor growth curves from individual mice treated with cisplatin or adoptive T cells alone or in the presence of LRG1 blocking antibody 15C4.

(**A**) Individual B16-F0 tumor growth rates in mice treated with IgG, 15C4, IgG plus cisplatin or 15C4 plus cisplatin (from mean data shown in Figure 5A). (**B**) Individual NP68-expressing B16-F10 tumor growth rates (from data shown in Figure 6A) of untreated mice or mice treated with control IgG, 15C4, IgG plus adoptive F5B6 cytotoxic T cells or 15C4 plus F5B6 T cells.

Supplemental Figure 6. B16-F0 tumor growth curves from individual mice treated with adoptive T cells or anti-PD1 alone or in the presence of LRG1 blocking antibody 15C4. (**A**) Individual growth curves of tumors (from Fig 6D) from mice bearing NP68-expressing B16-F10 subcutaneous tumors treated with F5B6 cytotoxic T cells and 15C4. (**B**) Immunohistochemical detection of CD3+ and donor T cell (CD90.2) infiltration into NP68-expressing B16-F10 subcutaneous tumors from mice treated with adoptive T cells alone or a combination of adoptive T cells and 15C4. Scale bar, 1 mm. (**C**) Individual growth curves of tumors (from Fig. 7A) from mice bearing B16-F0 subcutaneous tumors and treated with IgG control, IgG plus 15C4, IgG plus anti-PD1 and 15C4 plus anti-PD1.

Supplemental Figure 7. Effect of LRG1 inhibition on LLC tumor growth and immune cell infiltration and on B1-F0 HEV formation. A) Mean growth curves of LLC subcutaneous tumors from wild type mice treated with control IgG (n=34) 15C4 (n=32), anti-PD1 (n=32) and 15C4 plus anti-PD1 (n=32) (mean ± S.E.M). Growth curves analyzed by linear regression comparing pairs as shown, *P<0.05, **P<0.01, ****P<0.0001. (**B**) CD3+ and granzyme B+ T cell infiltration of LLC tumors. Scale bar 150 μm. Graphs show density (objects/mm^2) of CD3+ T cells (**C**) and granzyme B (**D**) from the different LLC treatment arms. Student t-test, *P<0.05, **P<0.01. (**E**) qPCR analysis of fold change in HEV signature genes in B16-F0 tumors from mice treated with control IgG, 15C4 plus IgG, anti-PD1 antibody and a combination of 15C4 and anti-PD1. N ≥ 3 samples per group. (**F**) Immunohistochemical staining of lymph node and B16-F0 tumors with an anti-CD31 antibody and the MECA79 antibody to detect PNAd. Tumors were taken from mice treated

with control IgG, 15C4, anti-PD1 antibody and a combination of 15C4 and anti-PD1. Scale

bar 50 µm.(**G**) Immunohistochemical staining of LLC tumors as in **F** above from mice treated

with control IgG, 15C4, anti-PD1 antibody and a combination of 15C4 and anti-PD1. Scale

bar 50 µm.

REFERENCES

1. Wang, X., Abraham, S., McKenzie, J.A., Jeffs, N., Swire, M., Tripathi, V.B., Luhmann, U.F., Lange, C.A., Zhai, Z., Arthur, H.M., Bainbridge, J.W., Moss S.E. and Greenwood, J. (2013). LRG1 promotes angiogenesis by modulating endothelial TGF-β signalling. Nature *499*, 306-311.

2. Hong, Q., Zhang, L., Fu, J., Verghese, D.A., Chauhan, K., Nadkarni, G.N., Li, Z., Ju, W., Kretzler, M., Cai, G.Y., Chen, X.M., D'Agati, V.D., Coca, S.G., Schlondorff, D., He, J.C. and Lee K. (2019). LRG1 promotes diabetic kidney disease progression by enhancing TGF-*β*-induced angiogenesis. J. Am. Soc. Nephrol. *30*, 546-562.

3. Folkman, J. (1971). Tumor angiogenesis: therapeutic implications. N. Engl. J. Med. *285*,1182-1186.

4. Hanahan, D. and Weinberg, R.A. (2011). Hallmarks of cancer: the next generation. Cell *144*, 646-674.

5. Carmeliet, P. and Jain, R.K. (2011). Principles and mechanisms of vessel normalization for cancer and other angiogenic diseases. Nat. Rev. Drug Discov. *10*, 417-427.

6. Wong, P.P., Bodrug, N. and Hodivala-Dilke, K.M. (2016). Exploring novel methods for modulating tumor blood vessels in cancer treatment. Curr. Biol. *26*, R1161-R1166.

7. Le Serve, A.W. and Hellmann, K. (1972). Metastases and the normalization of tumour blood vessels by ICRF 159: a new type of drug action. Br. Med. J. *4*, 597-601.

8. Jain, R.K. (2001). Normalizing tumor vasculature with anti-angiogenic therapy: a new paradigm for combination therapy. Nat. Med. *7*, 987–989.

9. Fukumura, D., Kloepper, J., Amoozgar, Z., Duda, D.G. and Jain, R.K. (2018). Enhancing cancer immunotherapy using antiangiogenics: opportunities and challenges. Nat. Rev. Clin. Oncol. *15*, 325-340.

10. Huang, Y., Yuan, J., Righi, E., Kamoun, W.S., Ancukiewicz, M., Nezivar, J., Santosuosso, M., Martin, J.D., Martin, M.R., Vianello, F., Leblanc, P., Munn, L.L., Huang, P., Duda, D.G., Fukumura, D., Jain, R.K. and Poznansky, M.C. (2012). Vascular

normalizing doses of antiangiogenic treatment reprogram the immunosuppressive tumor microenvironment and enhance immunotherapy. Proc. Natl. Acad. Sci. U.S.A. *109*,17561-17566.

11. Coutelle, O., Schiffmann, L.M., Liwschitz, M., Brunold, M., Goede, V., Hallek, M., Kashkar, H. and Hacker, U.T. (2015). Dual targeting of Angiopoetin-2 and VEGF potentiates effective vascular normalisation without inducing empty basement membrane sleeves in xenograft tumours. Br. J. Cancer *112*, 495-503.

12. Winkler, F., Kozin, S.V., Tong, R.T., Chae, S.S., Booth, M.F., Garkavtsev, I., Xu, L., Hicklin, D.J., Fukumura, D., di Tomaso, E., Munn, L.L. and Jain, R.K. (2004). Kinetics of vascular normalization by VEGFR2 blockade governs brain tumor response to radiation: role of oxygenation, angiopoietin-1, and matrix metalloproteinases. Cancer Cell *6*, 553-563.

13. El Alaoui-Lasmaili, K. and Faivre, B. (2018). Antiangiogenic therapy: Markers of response, "normalization" and resistance. Crit. Rev. Oncol. Hematol. *128*,118-129.

14. Allen, E., Jabouille, A., Rivera, L.B., Lodewijckx, I., Missiaen, R., Steri, V., Feyen, K., Tawney, J., Hanahan, D., Michael, I.P. and Bergers, G. (2017). Combined antiangiogenic and anti-PD-L1 therapy stimulates tumor immunity through HEV formation. Sci. Transl. Med. *9*, eaak9679.

15. Schmittnaegel, M., Rigamonti, N., Kadioglu, E., Cassará, A., Wyser Rmili, C., Kiialainen, A., Kienast, Y., Mueller, H.J., Ooi, C.H., Laoui, D. and De Palma, M. (2017). Dual angiopoietin-2 and VEGFA inhibition elicits antitumor immunity that is enhanced by PD-1 checkpoint blockade. Sci. Transl. Med. *9***,** eaak9670.

16. Johansson-Percival, A., He, B., Li, Z.J., Kjellén, A., Russell, K., Li, J., Larma, I. and Ganss, R. (2017). De novo induction of intratumoral lymphoid structures and vessel normalization enhances immunotherapy in resistant tumors. Nat. Immunol. *18*, 1207-1217.

17. Maes, H., Kuchnio, A., Peric, A., Moens, S., Nys, K., De Bock, K., Quaegebeur, A., Schoors, S., Georgiadou, M., Wouters, J., Vinckier, S., Vankelecom, H., Garmyn, M.,

Vion, A.C., Radtke, F., Boulanger, C., Gerhardt, H., Dejana, E., Dewerchin, M., Ghesquière, B., Annaert, W., Agostinis, P. and Carmeliet, P. (2014). Tumor vessel normalization by chloroquine independent of autophagy. Cancer Cell *26*, 190-206.

18. La Porta, S., Roth, L., Singhal, M., Mogler, C., Spegg, C., Schieb, B., Qu, X., Adams, R.H., Baldwin, H.S., Savant, S. and Augustin, H.G. (2018). Endothelial Tie1-mediated angiogenesis and vascular abnormalization promote tumor progression and metastasis. J. Clin. Invest. *128*, 834-845.

19. Munn, L.L. and Jain, R.K. (2019). Vascular regulation of antitumor immunity. Science *365*, 544-545.

20. Viallard, C. and Larrivée, B. (2017). Tumor angiogenesis and vascular normalization: alternative therapeutic targets. Angiogenesis *20*, 409-426.

21. Khan, K.A. and Kerbel, R.S. (2018). Improving immunotherapy outcomes with anti-angiogenic treatments and vice versa. Nat. Rev. Clin. Oncol. *15*, 310-324.

22. Martin, J.D., Seano, G. and Jain, R.K. (2019). Normalizing function of tumor vessels: Progress, opportunities, and challenges. Annu. Rev. Physiol. *81*, 505-534.

23. Huang, Y., Kim, B.Y.S., Chan, C.K. Hahn, S.M., Weissman, I.L. and Jiang, W. (2018). Improving immune-vascular crosstalk for cancer immunotherapy. Nat. Rev. Immunol. *18*, 195-203. (2018).

24. Schmittnaegel, M. and De Palma, M. (2017). Reprogramming tumor blood vessels for enhancing immunotherapy. Trends Cancer *3*, 809-812.

25. Tian, L., Goldstein, A., Wang, H., Ching Lo, H., Kim, I. Sun., Welte, T., Sheng, K., Dobrolecki, L.E., Zhang, X., Putluri, N., Phung, T.L., Mani, S.A., Stossi, F., Sreekumar, A., Mancini, M.A., Decker, W.K., Zong, C., Lewis, M.T. and Zhang, X.H. (2017). Mutual regulation of tumour vessel normalization and immunostimulatory reprogramming. Nature *544*, 250-254.

26. Johansson-Percival, A., He, B. and Ganss, R. (2018). Immunomodulation of tumor vessels: It takes two to tango. Trends Immunol. *39*, 801-814.

27. Andersen, J.D., Boylan, K.L., Jemmerson, R., Geller, M.A., Misemer, B., Harrington, K.M., Weivoda, S., Witthuhn, B.A., Argenta, P., Vogel, R.I. and Skubitz, A.P. (2010). Leucine-rich alpha-2-glycoprotein-1 is upregulated in sera and tumors of ovarian cancer patients. J. Ovarian Res. *3*, 21.

28. Sandanayake, N.S., Sinclair, J., Andreola, F., Chapman, M.H., Xue, A., Webster, G.J., Clarkson, A., Gill, A., Norton, I.D., Smith, R.C., Timms, J.F. and Pereira, S.P. (2011). A combination of serum leucine-rich alpha-2-glycoprotein 1, CA19-9 and interleukin-6 differentiate biliary tract cancer from benign biliary strictures. Br. J. Cancer *105*, 1370-1378.

29. Ladd, J.J., Busald, T., Johnson, M.M., Zhang, Q., Pitteri, S.J., Wang, H., Brenner, D.E., Lampe, P.D., Kucherlapati, R., Feng, Z., Prentice, R.L. and Hanash, S,M, (2012). Increased plasma levels of the APC-interacting protein MAPRE1, LRG1, and IGFBP2 preceding a diagnosis of colorectal cancer in women. Cancer Prev. Res. (Phila). *5*, 655-64

30. Wu, J., Xie, X., Nie, S., Buckanovich, R.J., and Lubman, D.M. (2013). Altered expression of sialylated glycoproteins in ovarian cancer sera using lectin-based ELISA assay and quantitative glycoproteomics analysis. J. Proteome Res. *12*, 3342-3352.

31. Wen, S.Y., Zhang, L.N., Yang, X.M., Zhang, Y.L., Ma, L., Ge, Q.L., Jiang, S.H., Zhu, X.L., Xu, W., Ding, W.J., Yang, B.Q., Zhang, Z.G. and Teng, Y.C. (2014). LRG1 is an independent prognostic factor for endometrial carcinoma. Tumour Biol. *35*, 7125-7133.

32. Wang, C.H., Li, M., Liu, L.L., Zhou, R.Y., Fu, J., Zhang, C.Z., and Yun, J.P. (2015). LRG1 expression indicates unfavorable clinical outcome in hepatocellular carcinoma. Oncotarget *6*, 42118-42129.

33. Sun, D.C., Shi, Y., Wang, L.X., Lv, Y., Han, Q.L., Wang, Z.K., and Dai, G.H. (2017). Leucine-rich alpha-2-glycoprotein-1, relevant with microvessel density, is an independent survival prognostic factor for stage III colorectal cancer patients: a retrospective analysis. Oncotarget *8*, 66550-66558.

34. Yamamoto, M., Takahashi, T., Serada, S., Sugase, T., Tanaka, K., Miyazaki, Y., Makino, T., Kurokawa, Y., Yamasaki, M., Nakajima, K., Takiguchi, S., Naka, T., Mori, M. and Doki, Y. (2017). Overexpression of leucine-rich alpha2-glycoprotein-1 is a prognostic marker and enhances tumor migration in gastric cancer. Cancer Sci *108*, 2052-2060.

35. Zhang, Q., Huang, R., Tang, Q., Yu, Y., Huang, Q., Chen, Y., Wang, G., and Wang, X. (2018). Leucine-rich alpha-2-glycoprotein-1 is up-regulated in colorectal cancer and is a tumor promoter. Onco. Targets Ther. *11*, 2745-2752.

36. Wang, Y., Xing, Q., Chen, X., Wang, J., Guan, S., Chen, X., Sun, P., Wang, M. and Cheng, Y. (2019). The Clinical Prognostic Value of LRG1 in Esophageal Squamous Cell Carcinoma. Curr. Cancer Drug Targets. *19*, 756-763.

37. Guldvik, I.J., Zuber, V., Braadland, P.R., Grytli, H.H., Ramberg, H., Lilleby, W., Thiede, B., Zucknick, M., Saatcioglu, F., Gislefoss, R., Kvåle, R., George, A., Grönberg, H., Wiklund, F., Neal, D.E., Gnanapragasam, V.J., Taskén, K.A. and, Mills, I.G. (2020). Identification and Validation of Leucine-rich alpha-2-glycoprotein 1 as a Noninvasive Biomarker for Improved Precision in Prostate Cancer Risk Stratification. Eur. Urol. Open Sci. *21*, 51-60.

38. Jin, Z., Kobayashi, S., Gotoh, K., Takahashi, T., Eguchi, H., Naka, T., Mori, M. and Doki, Y. (2020). The Prognostic Impact of Leucine-Rich alpha-2-Glycoprotein-1 in Cholangiocarcinoma and Its Association With the IL-6/TGF-beta1 Axis. J. Surg. Res. *252*, 147-155.

39. Zhang, Y.S., Han, L., Yang, C., Liu, Y.J. and Zhang, X.M. (2021). Prognostic Value of LRG1 in Breast Cancer: A Retrospective Study. Oncol. Res. Treat. *44*, 36-42.

40. Gopinathan, A., Morton, J.P., Jodrell, D.I. and Sansom, O.J. (2015). GEMMs as preclinical models for testing pancreatic cancer therapies. Dis. Model. Mech. *8*,1185-1200.

41. Gerhardt, H. and Betsholtz, C. (2003). Endothelial-pericyte interactions in angiogenesis. Cell Tissue Res. *314*, 15-23.

42. De Bock, K., Cauwenberghs, S. and Carmeliet, P. (2011). Vessel abnormalization: another hallmark of cancer? Molecular mechanisms and therapeutic implications. Curr. Opin. Genet. Dev. *21*, 73–79.

43. Hashizume, H., Baluk, P., Morikawa, S., McLean, J.W., Thurston, G., Roberge, S. Jain, R.K. and McDonald, D.M. (2000). Openings between defective endothelial cells explain tumor vessel leakiness. Am. J. Pathol. *156*,1363-1380.

44. Kallenberg, D., Tripathi, V., Javaid, F., Pilotti, C., George, J., Davis, S., Blackburn, J.W.D., O'Connor, M., Dowsett, L., Bowers, C.E., Liyanage, S., Gourlaouen, M., Hoeh, A., Mota, F., Selwood, D., Bainbridge, J., Tufail, A., Chudasama, V., Greenwood, J. and Moss, S.E. (2020). A humanized antibody against LRG1 that inhibits angiogenesis and reduces retinal vascular leakage.
bioRxiv 2020.07.25.218149; doi: https://doi.org/10.1101/2020.07.25.218149

45. Giannotta, M., Trani, M. and Dejana, E. (2013). VE-cadherin and endothelial adherens junctions: active guardians of vascular integrity. Dev. Cell *26*, 441-454.

46. Li, X., Kumar, A. and Carmeliet, P. (2019). Metabolic pathways fueling the endothelial cell drive. Annu. Rev. Physiol. *81*, 483-503.

47. Schoors, S., De Bock, K., Cantelmo, A.R., Georgiadou, M., Ghesquière, B., Cauwenberghs, S., Kuchnio, A., Wong, B.W., Quaegebeur, A., Goveia, J., Bifari, F., Wang, X., Blanco, R., Tembuyser, B., Cornelissen, I., Bouché, A., Vinckier, S., Diaz-Moralli, S., Gerhardt, H., Telang, S., Cascante, M., Chesney, J., Dewerchin, M. and Carmeliet, P. (2014). Partial and transient reduction of glycolysis by PFKFB3 blockade reduces pathological angiogenesis. Cell Metab. *19*, 37-48.

48. Watson, H.A., Dolton, G., Ohme, J., Ladell, K., Vigar, M., Wehenkel, S., Hindley, J., Mohammed, R.N., Miners, K., Luckwell, R.A., Price, D.A., Matthews, R.J. and Ager, A. (2016). Purity of transferred CD8(+) T cells is crucial for safety and efficacy of combinatorial tumor immunotherapy in the absence of SHP-1. Immunol. Cell Biol. *94*, 802-808.

49. Bertrand, F., Montfort, A., Marcheteau, E., Imbert, C., Gilhodes, J., Filleron, T., Rochaix,

P., Andrieu-Abadie, N., Levade, T., Meyer, N., Colacios, C. and, Ségui, B. (2017). TNFα blockade overcomes resistance to anti-PD-1 in experimental melanoma. Nat. Commun. *8*, 2256.

50. Li, H.Y., McSharry, M., Bullock, B., Nguyen, T.T., Kwak, J., Poczobutt, J.M., Sippel, T.R., Heasley, L.E., Weiser-Evans, M.C., Clambey, E.T. and Nemenoff, R.A. (2017). The Tumor Microenvironment Regulates Sensitivity of Murine Lung Tumors to PD-1/PD-L1 Antibody Blockade. Cancer Immunol. Res. *9*, 767-777.

51. Lin, H., Wei, S., Hurt, E.M., Green, M.D., Zhao, L., Vatan, L., Szeliga, W., Herbst, R., Harms, P.W., Fecher, L.A., Vats, P., Chinnaiyan, A.M., Lao, C.D., Lawrence, T.S., Wicha, M., Hamanishi, J., Mandai, M., Kryczek, I. and Zou, W. (2018). Host expression of PD-L1 determines efficacy of PD-L1 pathway blockade-mediated tumor regression. J. Clin. Invest. *128*, 805-815.

52. Allen, E., Missiaen, R. and Bergers, G. (2017). Therapeutic induction of high endothelial venules (HEVs) to enhance T-cell infiltration in tumors. Oncotarget *8*, 99207-99208.

53. Shirai, R., Hirano, F., Ohkura, N., Ikeda, K. and Inoue, S. (2009). Up-regulation of the expression of leucine-rich alpha(2)-glycoprotein in hepatocytes by the mediators of acute-phase response. Biochem. Biophys. Res. Commun. *382*, 776-779.

54. Liu, C., Yen Teo, M.H., Ting Pek, S.L., Wu, X., Leong, M.L., Tay, H.M., Hou, H.W., Ruedl, C., Moss, S.E., Greenwood, J., Tavintharan, S., Hong, W. and Wang, X. (2020). A multifunctional role of leucine-rich-alpha 2 glycoprotein 1 in cutaneous wound healing under normal and diabetic conditions. Diabetes *69*, 2467-2480.

55. Gao, Y., Xie, Z., Ho, C., Wang, J., Li, Q., Zhang, Y. and Zhou, J. (2020). LRG1 Promotes Keratinocyte Migration and Wound Repair through Regulation of HIF-1alpha Stability. J. Invest. Dermatol. *140*, 455-464 e458

56. Bergers, G. and Song, S. (2005). The role of pericytes in blood-vessel formation and maintenance. Neuro. Oncol. *7*, 452-464.

57. Dekker, R.J., Boon, R.A., Rondaij, M.G., Kragt, A., Volger, O.L., Elderkamp, Y.W., Meijers, J.C., Voorberg, J., Pannekoek, H. and Horrevoets, A.J. (2006). KLF2 provokes

a gene expression pattern that establishes functional quiescent differentiation of the endothelium. Blood *107*, 4354-4363.

58. Egorova, A.D., Van der Heiden, K., Van de Pas, S., Vennemann, P., Poelma, C., DeRuiter, M.C., Goumans, M.J., Gittenberger-de Groot, A.C., ten Dijke, P., Poelmann, R.E. and Hierck, B.P. (2011). Tgfβ/Alk5 signaling is required for shear stress induced klf2 expression in embryonic endothelial cells. Dev. Dyn. *240*, 1670-1680.

59. Park, B.V., Freeman, Z.T., Ghasemzadeh, A., Chattergoon, M.A., Rutebemberwa, A., Steigner, J., Winter, M.E., Huynh, T.V., Sebald, S.M., Lee, S.J., Pan, F., Pardoll, D.M. and Cox, A.L. (2016). TGFβ1-Mediated SMAD3 Enhances PD-1 Expression on Antigen-Specific T Cells in Cancer. Cancer Discov. *6*, 1366-1381.

60. Tang, P.M., Zhou, S., Meng, X.M., Wang, Q.M., Li, C.J., Lian, G.Y., Huang, X.R., Tang, Y.J., Guan, X.Y., Yan, B.P., To, K.F. and Lan, H.Y. (2017). Smad3 promotes cancer progression by inhibiting E4BP4-mediated NK cell development. Nat. Commun. *8*:14677.

61. Zeng, Q., Li, S., Chepeha, D.B., Giordano, T.J., Li, J., Zhang, H., Polverini, P.J., Nor, J., Kitajewski, J. and Wang, C.Y. (2005). Crosstalk between tumor and endothelial cells promotes tumor angiogenesis by MAPK activation of Notch signaling. Cancer Cell. *8*, 13-23.

62. Graeber, T.G., Osmanian, C., Jacks, T., Housman, D.E., Koch, C.J., Lowe, S.W. and Giaccia, A.J. (1996). Hypoxia-mediated selection of cells with diminished apoptotic potential in solid tumours. Nature *379*, 88-91.

63. Anderson, A.R., Weaver, A.M., Cummings, P.T. and Quaranta, V. (2006). Tumor morphology and phenotypic evolution driven by selective pressure from the microenvironment. Cell *127*, 905-915.

64. McIntyre, A. and Harris, A.L. (2015). Metabolic and hypoxic adaptation to anti-angiogenic therapy: a target for induced essentiality. EMBO Mol. Med. *7*, 368-379.

65. Terry, S., Faouzi Zaarour, R., Hassan Venkatesh, G., Francis, A., El-Sayed, W., Buart, S., Bravo, P., Thiery, J. and Chouaib, S. (2018). Role of hypoxic stress in regulating tumor immunogenicity, resistance and plasticity. Int. J. Mol. Sci. *19*, 3044.

66. Xie, Z.B., Zhang, Y.F., Jin, C., Mao, Y.S. and Fu, D.L. (2019). LRG-1 promotes pancreatic cancer growth and metastasis via modulation of the EGFR/p38 signaling. J. Exp. Clin. Cancer Res. *38*, 75.

67. Takemoto, N., Serada, S., Fujimoto, M., Honda, H., Ohkawara, T., Takahashi, T., Nomura, S., Inohara, H. and Naka, T. (2015). Leucine-rich α-2-glycoprotein promotes TGFβ1-mediated growth suppression in the Lewis lung carcinoma cell lines. Oncotarget. *6*, 11009-11022.

68. Singhal, M., Gengenbacher. N., Pari. A.A.A., Kamiyama, M., Hai. L., Kuhn, B.J., Kallenberg, D.M., Kulkarni, S.R., Camilli, C., Preu, S.F., Leuchs, B., Mogler, C., Espinet, E., Besemfelder, E., Heide, D., Heikenwalder, M., Sprick, M.R., Trumpp, A., Krijgsveld, J., Schlesner, M., Hu, J., Moss, S.E., Greenwood, J. and Augustin, H.G. (2021). Temporal multi-omics identifies LRG1 as a vascular niche instructor of metastasis. Sci Trans Med. Sep;13(609):eabe6805. doi: 10.1126/scitranslmed.abe6805. Epub 2021 Sep 1

69. Kwan, Y.P., Teo, M.H.Y., Lim, J.C.W., Tan, M.S., Rosellinny, G., Wahli, W. and Wang, X. (2021). LRG1 Promotes Metastatic Dissemination of Melanoma through Regulating EGFR/STAT3 Signalling. Cancers (Basel). *13*, 3279.

70. Wohlkoenig, C., Leithner, K., Deutsch, A., Hrzenjak, A., Olschewski, A. and Olschewski, H. (2011). Hypoxia-induced cisplatin resistance is reversible and growth rate independent in lung cancer cells. Cancer Lett. *308*, 134-143.

71. Watson, H.A., Durairaj, R.R.P., Ohme, J., Alatsatianos, M., Almutairi, H., Mohammed, R.N., Vigar, M., Reed, S.G., Paisey, S.J., Marshall, C., Gallimore, A. and Ager, A. (2019). L-selectin enhanced T cells improve the efficacy of cancer immunotherapy. Front. Immunol. *10*, 1321.

72. Shrimali, R.K., Yu, Z., Theoret, M.R., Chinnasamy, D., Restifo, N.P. and Rosenberg, S.A. (2010). Antiangiogenic agents can increase lymphocyte infiltration into tumor and enhance the effectiveness of adoptive immunotherapy of cancer. Cancer Res. *70*, 6171-6180.

73. Slaney, C.Y., Kershaw, M.H. and Darcy, P.K. (2014). Trafficking of T cells into tumors. Cancer Res. *74*, 7168-7174.

74. Ager, A., Watson, H.A., Wehenkel, S.C. and Mohammed, R.N. (2016). Homing to solid cancers: a vascular checkpoint in adoptive cell therapy using CAR T-cells. Biochem. Soc. Trans. *44*, 377-385.

75. Zou, W., Wolchok, J.D. and Chen, L. (2016). PD-L1 (B7-H1) and PD-1 pathway blockade for cancer therapy: Mechanisms, response biomarkers, and combinations. Sci. Transl. Med. *8*, 328rv4.

76. Galon, J. and Bruni, D. (2019). Approaches to treat immune hot, altered and cold tumours with combination immunotherapies. Nat. Rev. Drug Discov. *18*, 197-218.

77. O'Donnell, J.S., Teng, M.W. and Smyth, M.J. (2018). Cancer immunoediting and resistance to T cell-based immunotherapy. Nat. Rev. Clin. Oncol. *16*, 151-167.

78. Griffioen, A.W., Damen, C.A., Blijham, G.H. and Groenewegen, G. (1996). Tumor angiogenesis is accompanied by a decreased inflammatory response of tumor-associated endothelium. Blood *88*, 667–673.

79. Griffioen, A.W., Damen, C.A., Martinotti, S., Blijham, G.H. and Groenewegen, G. (1996). Endothelial intercellular adhesion molecule-1 expression is suppressed in human malignancies: the role of angiogenic factors. Cancer Res. *56*, 1111–1117.

80. Piali, L., Fichtel, A., Terpe, H.J., Imhof, B.A. and Gisler, R.H. (1995). Endothelial vascular cell adhesion molecule 1 expression is suppressed by melanoma and carcinoma. J. Exp. Med. *181*, 811–816.

81. Joyce, J.A. and Fearon, D.T. (2015). T cell exclusion, immune privilege, and the tumor microenvironment. Science *348*, 74-80.

82. Klein, D. (2018). The tumor vascular endothelium as decision maker in cancer therapy. Front. Oncol. *8*, 367.

83. Tual-Chalot, S., Garcia-Collado, M., Redgrave, R.E., Singh, E., Davison, B., Park, C., Lin, H., Luli, S., Jin, Y., Wang, Y., Lawrie, A., Jakobsson, L. and Arthur, H.M. (2020). Loss of endothelial endoglin promotes high-output heart failure through peripheral

arteriovenous shunting driven by VEGF signaling. Circ. Res. *126,* 243-257.

84. Moser, A.R., Luongo, C., Gould, K.A., McNeley, M.K., Shoemaker, A.R. and Dove, W.F. (1995). ApcMin: a mouse model for intestinal and mammary tumorigenesis. Eur. J. Cancer. *31A*, 1061-1064.

85. Hingorani, S.R., Wang, L., Multani, A.S., Combs, C., Deramaudt, T.B., Hruban, R.H., Rustgi, A.K., Chang, S. and Tuveson, D.A. (2005). Trp53R172H and KrasG12D cooperate to promote chromosomal instability and widely metastatic pancreatic ductal adenocarcinoma in mice. Cancer Cell. *7*, 469-483.

86. el Marjou, F., Janssen, K.P., Chang, B.H., Li, M., Hindie, V., Chan, L., Louvard, D., Chambon, P., Metzger, D. and Robine, S. (2004). Tissue-specific and inducible Cre-mediated recombination in the gut epithelium. Genesis. *39*,186-193.

87. Shibata, H., Toyama, K., Shioya, H., Ito, M., Hirota, M., Hasegawa, S., Matsumoto, H., Takano, H., Akiyama, T., Toyoshima, K., Kanamaru, R., Kanegae, Y., Saito, I., Nakamura, Y., Shiba, K. and Noda, T. (1997). Rapid colorectal adenoma formation initiated by conditional targeting of the Apc gene. Science. *278*, 120-123.

KEY RESOURCES TABLE

REAGENT or RESOURCE	SOURCE	IDENTIFIER
Antibodies		
Rabbit polyclonal anti-CD31	Abcam	Cat#ab28364; RRID: AB_726362
Rat monoclonal anti-CD31	Dianova	Cat#DIA-310; RRID: AB_726362
Goat polyclonal anti-podocalyxin	R&D Systems	Cat3#AF1556; RRID: AB_354858
Mouse monoclonal anti-VE-cadherin	Santa Cruz	Cat#SC9989; RRID: AB_2077957
Rat monoclonal anti-endomucin	Abcam	Cat#ab106100; RRID: AB_10859306
Rabbit polyclonal anti-NG2	Merck-Millipore	Cat#AB5320; RRID: AB_11213678
Mouse monoclonal anti-αSMA	Sigma-Aldrich	Cat#C6198; RRID: AB_476856
Goat polyclonal anti-collagen-IV	Merck-Millipore	Cat#AB769; RRID: AB_92262
Mouse monoclonal anti-perlecan	Abcam	Cat#ab23418; RRID: Not known
Rabbit polyclonal anti-CD3	Abcam	Cat#ab5690; RRID: AB_305055
Rat Monoclonal anti-CD8a (YTS105.18)	Novus	Cat#NB200-578; RRID: Not known
Rat monoclonal anti-CD90.2	Biolegend	Cat#105301; RRID: AB_313173
Goat polyclonal anti-Granzyme B	R&D Systems	Cat#AF1865; RRID: AB_2294988
Monoclonal anti-MECA-79 AlexaFluor 488	EBioscience	Cat#53-6036-80
FITC-labelled Lycopersicon esculentum lectin	Vector labs	Cat#FL-1171
Hoechst 33342	Sigma-Aldrich	Cat#14533
gamma-H2AX	Merck-Millipore	Cat#05-636
Mouse monoclonal anti-LRG1 15C4	This paper	N/A
Rabbit polyclonal antibody anti-LRG1	Atlas Antibodies	Cat#HPA001888
Rabbit polyclonal antibody anti-LRG1	Proteintech	13224-1-AP
IgG1	Bio X Cell	Cat#BE0083
IgG2a	Bio X Cell	Cat#BE0089
Rat monoclonal anti-PD1 (CD279)	Bio X Cell	Cat#BP0146; RRID: AB_10949053
CD45 MicroBeads	Miltenyi Biotec	Cat#130-110-618
Rat monoclonal anti-CD31-FITC	Biolegend	Cat#102405; RRID: AB_312900
EF5 Hypoxia Detection Kit, Cyanine 3	Merck-Millipore	Cat#EF5-30C3
Goat anti-rabbit HRP	Dako	Cat#P0448
Rabbit polyclonal anti-pAkt(Ser473)	Cell Signaling	Cat#4060; RRID: AB_2315049
Rabbit polyclonal anti-Akt	Cell Signaling	Cat#9272; RRID: AB_329827
Rabbit monoclonal anti-pErk1/2	Cell Signaling	Cat#4370; RRID: AB_2315112

Rabbit polyclonal anti-Erk1/2	Cell Signaling	Cat#9102; RRID: AB_330744
Mouse monoclonal anti-pSapk/Jnk	Cell Signaling	Cat#9255; RRID: AB_2307321
Rabbit polyclonal anti-Sapk/Jnk	Cell Signaling	Cat#9252; RRID: AB_2250373
Rabbit polyclonal anti-phospho-p38 MAPK	Cell Signaling	Cat#9211; RRID: AB_331641
Rabbit polyclonal anti-p38 MAPK	Cell Signaling	Cat#9212; RRID: AB_330713
Rabbit monoclonal anti-pSmad3	Cell Signaling	Cat#9520; RRID: AB_2193207
Rabbit monoclonal anti-Smad2/3	Cell Signaling	Cat#8685; RRID: AB_10889933
Mouse monoclonal anti-GAPDH	ProteinTech	Cat#60004-1-Ig; RRID: AB_2107436
Human IgG4	Abcam	Cat#ab90286; RRID: AB_11040692
Bacterial and virus strains		
Biological samples		
Human lung cancer	Proteogenex Inc. California, USA (https://www.proteogenex.com	Cat#042471T2
Human prostate cancer	Amsbio (https://www.amsbio.com)	Cat#TP241b
Human breast carcinoma	Pantomics (https://www.pantomics.com)	Cat#MTU951
Human NSCLC serum samples	Proteogenex, Inc. California, USA, (https://www.proteogenex.com)	Cat#F88-3203351
Human CRC serum samples	Proteogenex, Inc. California, USA (https://www.proteogenex.com)	Cat#F88-3203351
Human pancreatic cancer serum samples	Proteogenex, Inc. California, USA (https://www.proteogenex.com)	Cat#F88-3203351
Human normal donor serum samples	Proteogenex, Inc. California, USA (https://www.proteogenex.com)	Cat#F88-3203351
Chemicals, peptides, and recombinant proteins		
Tamoxifen	Sigma	T5648
Corn oil	Sigma	C8267
4% Paraformaldehyde	TAAB	F003
Formalin	Genta Medical	BFN025
NP68 (ASNENMDAM)	Peptide Synthetics	Custom order
Incomplete Freund's adjuvant	Sigma	F5506
Hexamethyldisilazane	Aldrich chemicals	440191

Cisplatin	Accord	N/A
BOND Epitope Retrieval Solution 2	Leica	AR9640
Critical commercial assays		
RNAScope 2.0 HD Detection kit – BROWN	Advanced Cell Diagnostics	320497
RNAScope Multiplex Fluorescent Kit v2	Advanced Cell Diagnostics	323100
TSA® signal amplification	PerkinElmer	NEL744001KT
ApopTag in situ apoptosis detection kit	Merck-Millipore	s7110
RNeasy mini/midi kit	Qiagen	74106/75144
LunaScript RT SuperMix Kit	New England Biolabs	E3010
ELISA substrate reagent kit	R&D Systems	DY999
FluoroTag conjugation kit	Sigma-Aldrich	FITC1
Dako Envision+ system HRP labeled polymer anti-rabbit	Dako	K4002
Deposited data		
RNASeq data from B16-F0 tumors from WT and *Lrg1* knockout mice	This paper	NCBI Sequence Read Archive https://www.ncbi.nlm.nih.gov/sra/PRJNA552723
RNASeq data from B16-F0 tumor vessels from control and 15C4 treated mice	This paper	NCBI Gene Expression Omnibus https://www.ncbi.nlm.nih.gov/geo/query/acc.cgi?acc=GSE184816
Experimental models: Cell lines		
B16-F0 (mouse melanoma)	ATCC	CRL-6322
LLC1 (LL/2; mouse Lewis Lung carcinoma)	ATCC	CRL-1642
NP68-B16 (mouse melanoma expressing NP68 peptide	Watson et al, 2019[71]	PMID: 31249570
Experimental models: Organisms/strains		
Mouse: C57BL/6J	Harlan & Charles River Laboratories	N/A
Mouse: C57BL/6N	Charles River Laboratories	N/A
Mouse: C57BL/6.PL-Thy1a (Thy1.1/CD90.1)	Jackson Laboratory	N/A
Mouse: *Lrg1*−/−	University of California Davis knockout mouse project (KOMP) repository (http://www.komp.org/)	N/A
Mouse: *Apc*Min	Moser et al. 1995[84]	PMID: 7576992
Mouse: *Pdx1-Cre; Kras*LSL-G12D/+*;Trp53*LSL-R172H/+*(KPC)*	Hingorani et al. 2005[85]	PMID: 15894267
Mouse: *villin*CreER	el Marjou et al. 2004[86]	PMID: 15282745
Mouse: *Apc* (floxed)	Shibata et al., 1997[87]	PMID: 9311916
Oligonucleotides		
Ccl19, Forward: CAGTCACTCCCCTGTGAACC, Reverse: CAGAGTTGGGGCTGGGAAG	Life technologies	N/A
Ccl21a, Forward: AAGGCAGTGATGGAGGGGGT, Reverse: CTTAGAGTGCTTCCGGGGTG,	Life technologies	N/A
Cxcl13, Forward: CAGGCCACGGTATTCTGGA, Reverse: CAGGGGGCGTAACTTGAATC	Life technologies	N/A
Glycam1, Forward: TCAGCTGCAACCACCTCAG, Reverse: TTCGTGATACGACTGGCACC	Life technologies	N/A

Software and algorithms		
NIS-Elements software	Nikon	N/A
ImageJ	http://imagej.nih.gov/ij/	N/A
RT-qPCR on QuantStudio 6	Applied Biosciences	N/A
Luna Universal qPCR kit	New England Biolabs	M3003
Graphpad Prism version 5.0 or 7.0 for Windows, GraphPad Software, www.graphpad.com	La Jolla California USA	N/A
Other		
Dako fluorescent mounting medium	Agilent	S3023
ProLong™ Gold Antifade Mountant	Fisher Scientific	11539306
Dulbecco's Modified Eagle's Medium	Thermofisher Scientific	21969035

Figure 1
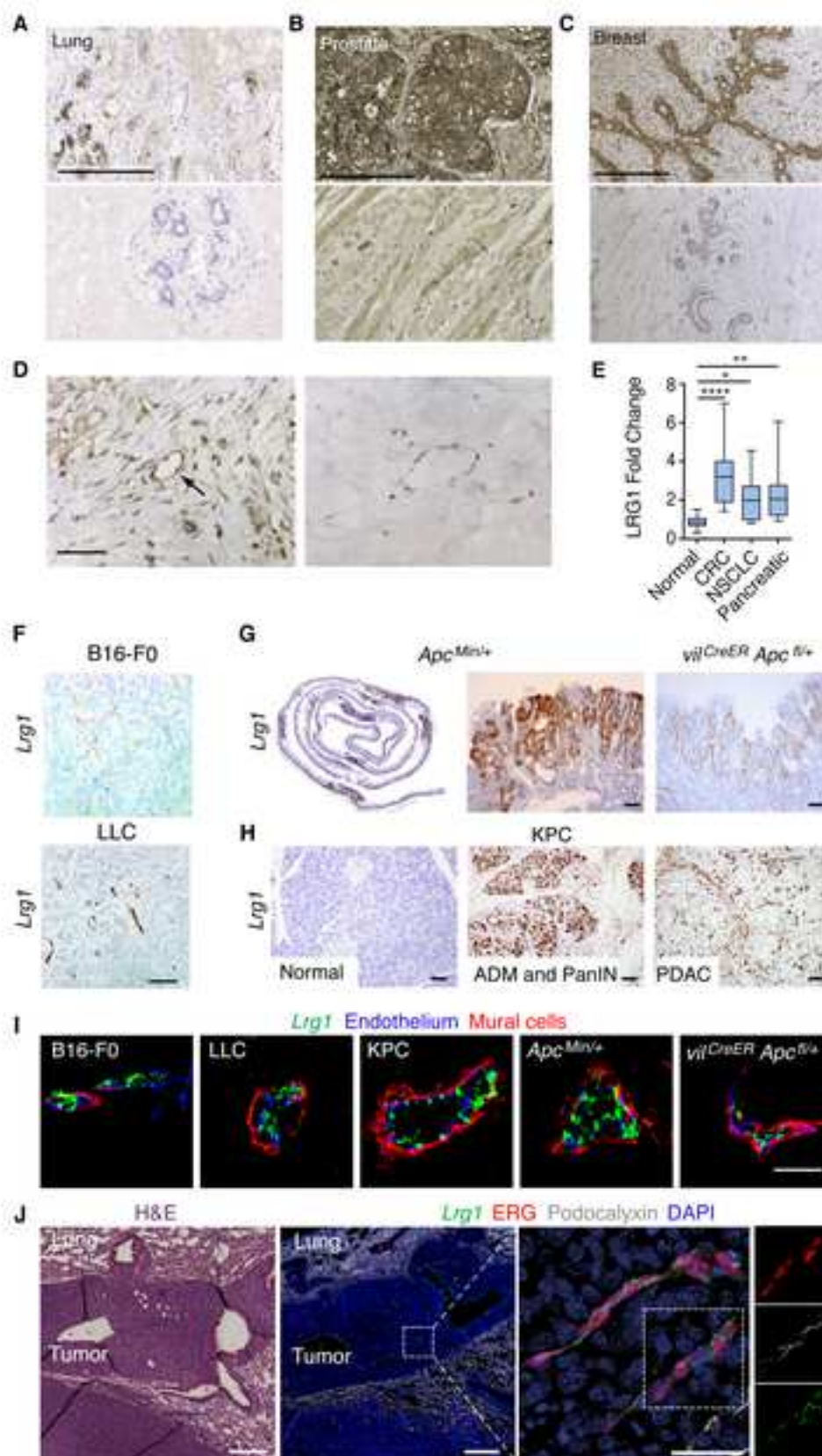
Figure 2
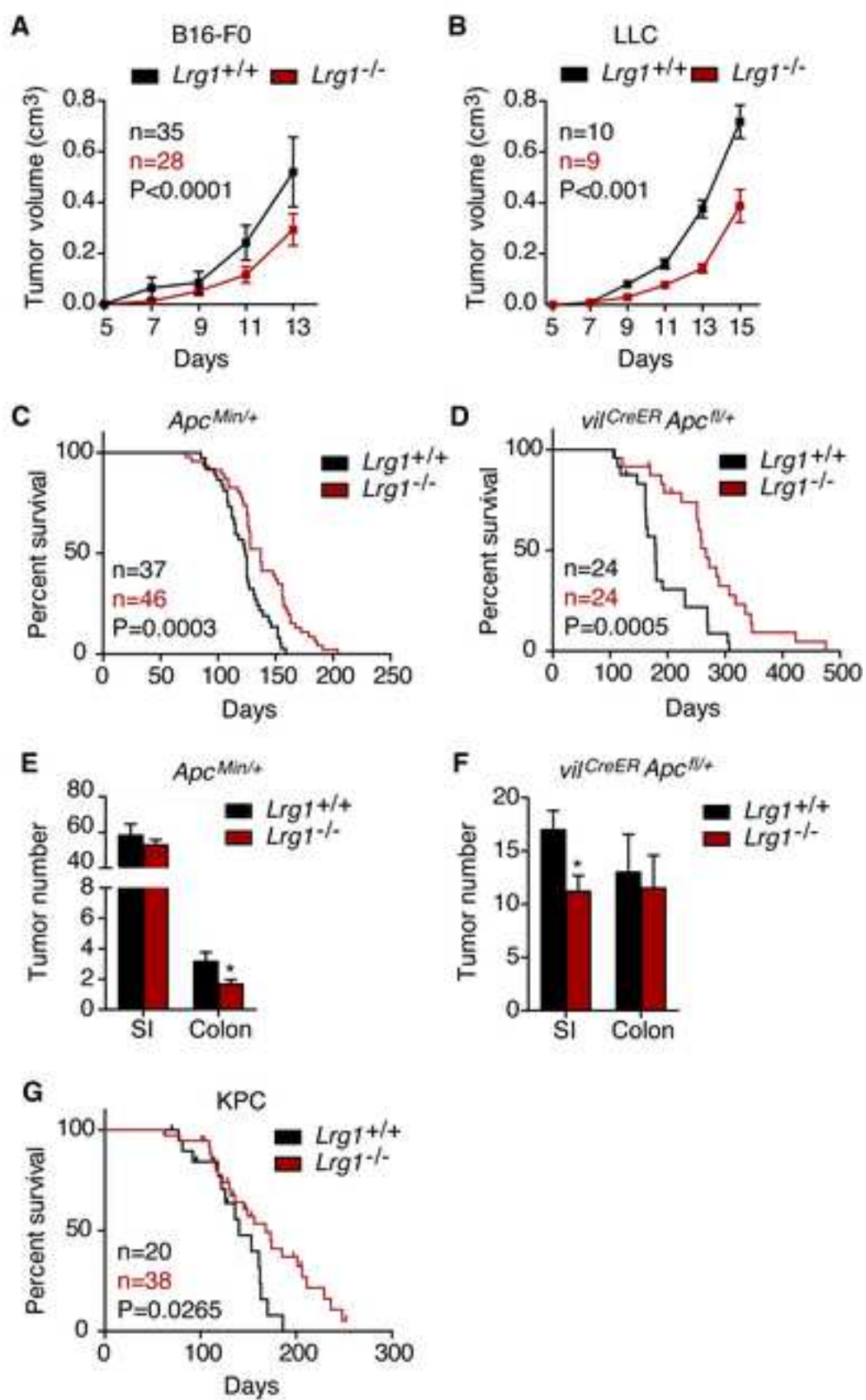
Figure 3
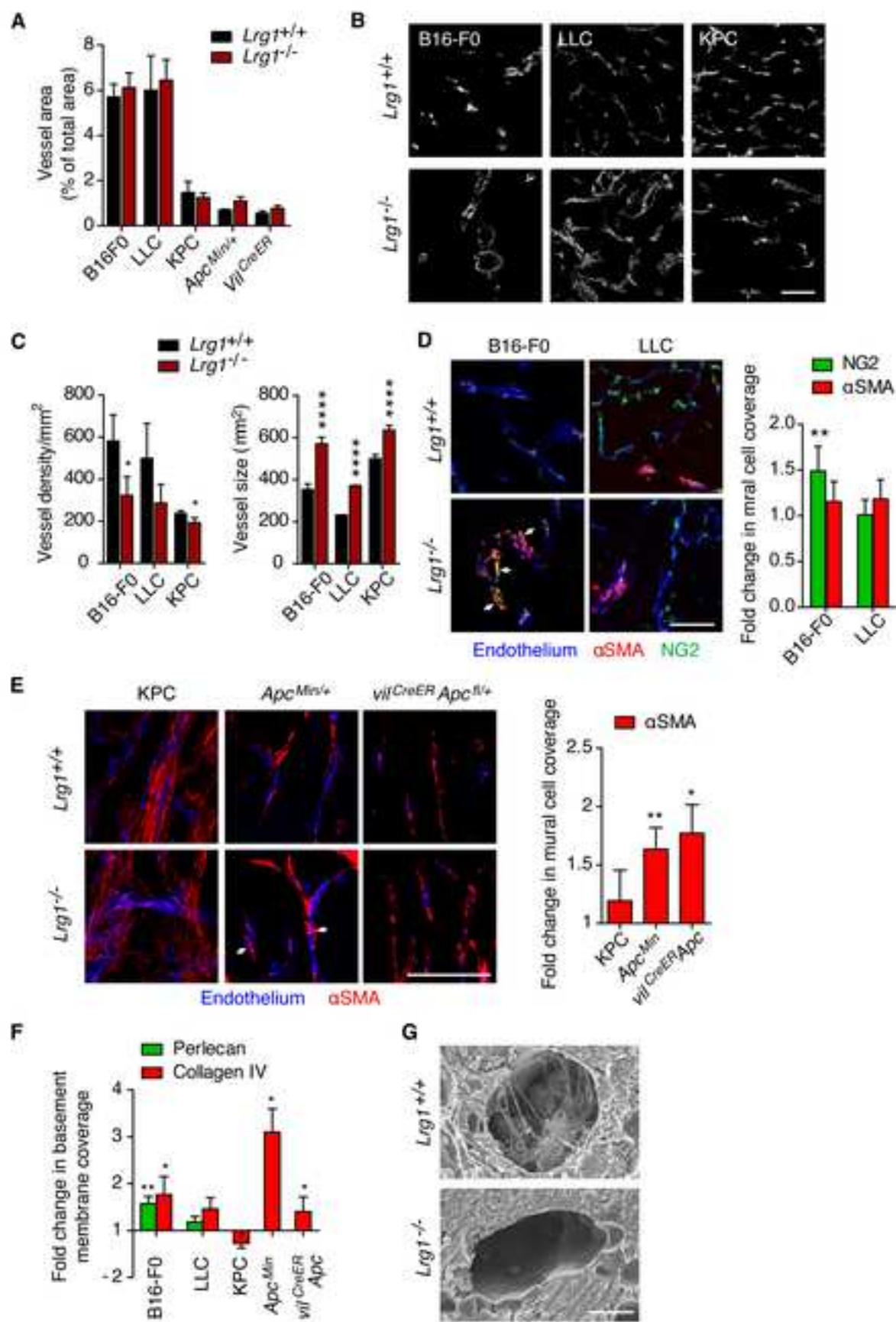
Figure 4

Figure 5

Figure 6

A Tumor volume (cm³) vs Days after B16 implantation
- No Transfer
- IgG
- 15C4
- IgG + F5B6
- 15C4 + F5B6

B Mean growth rate

C No transfer / IgG + F5B6 / 15C4 + F5B6
- Total T-cells
- Donor T-cells
- Endothelium

CD3⁺ objects/mm²
CD90.2⁺ objects/mm²

D Tumor volume (cm³) vs Days post tumor transfer
- No Transfer
- IgG + F5B6
- 15C4 + F5B6

CD3⁺ objects/mm²
CD90.2⁺ objects/mm²

Figure 7

A Skin / Pancreas / Small intestine — *Ppib* (green), Endothelium (red), Nuclei (blue), Merge

B Skin / Pancreas / Small intestine — *Lrg1* (green), Endothelium (red), Nuclei (blue), Merge

C s.c. inoculation of LLC cells → Primary tumor-resection → Survival endpoint; Perioperative 15C4 treatment

D *Lrg1* ERG Podocalyxin DAPI — WT Liver, *Lrg1⁻/⁻* Liver, Lung

Supplemental Figure 1

A B16-F0

Lrg1⁺/⁺ *Lrg1⁻/⁻*

B LLC

Lrg1⁺/⁺ *Lrg1⁻/⁻*

C *Apc^Min/+* *vil^CreER Apc^fl/+*

Lrg1⁺/⁺

Lrg1⁻/⁻

D B16-F0 LLC KPC *Apc^Min/+* *vil^CreER Apc^fl/+*

Lrg1⁺/⁺

Lrg1⁻/⁻

Endothelium
Perlecan   Collagen IV

Endothelium   Collagen IV

E B16-F0 IgG B16-F0 15C4

F B16-F0 IgG 15C4

Vessel area (% of total area)   Vessel density/mm²   Vessel size (mm²)

G B16-F0 IgG 15C4

IgG   15C4

Overlap with CD31 relative to wild type (%)

Perlecan   Coll.IV

Endothelium
Perlecan   Collagen IV

Supplemental Figure 2

Supplemental Figure 3

A

p-AKT
Total AKT
p-ERK1/2
Total ERK1/2
p-SAPK/JNK
Total SAPK/JNK
p-p38
Total p38
GAPDH

IgG   15C4

p-AKT/total AKT   **
p-ERK/total ERK   *
p-JNK/total JNK
p-p38/total p38

B

p-Smad3
Total Smad2/3
GAPDH

IgG   15C4

p-Smad3/total Smad 2/3   *

C

Icam1   *P* < 0.0112
Icam2
Vcam1   *P* < 0.0076
Pecam1
Sele
Selp
Jam2
Jam3

log2FC

Supplemental Figure 4

A

IgG

15C4

IgG + cisplatin

15C4 + cisplatin

B

No transfer

IgG

15C4

IgG + F5B6

15C4 + F5B6

Supplemental Figure 5

A

| No transfer | IgG + F5B6 | 15C4 + F5B6 |

Tumor volume (cm³) vs *Days Post Tumor Injection*

B

| | CD3 | CD90.2 | Endothelium | Merge |

IgG + F5B6

15C4 + F5B6

C

| IgG | IgG + 15C4 |
| IgG + anti-PD1 | 15C4 + anti-PD1 |

Tumor volume (cm³) vs *Days after B16 inoculation*

Supplemental Figure 6

A

- IgG
- 15C4
- αPD1
- 15C4 + αPD1

Tumor volume (cm^3)

Days after LLC implantation

B

IgG | 15C4
PD1 | 15C4 + αPD1

CD3 Granzyme B

C

CD3$^+$ object density/mm^2

IgG | 15C4+IgG | αPD1 | 15C4+αPD1

D

Granzyme B object density/mm^2

IgG | 15C4+IgG | αPD1 | 15C4+αPD1

E

Glycam1

2^(ΔΔCt)

IgG | 15C4+IgG | αPD1 | 15C4+αPD1

Ccl19

2^(ΔΔCt)

IgG | 15C4+IgG | αPD1 | 15C4+αPD1

Ccl21a

2^(ΔΔCt)

IgG | 15C4+IgG | αPD1 | 15C4+αPD1

Cxcl13

2^(ΔΔCt)

IgG | 15C4+IgG | αPD1 | 15C4+αPD1

F

CD31 | MECA79 | Merge

Control lymph node

B16-F0 tumor

IgG

15C4

PD-1

15C4 + PD-1

G

CD31 | MECA79 | Merge DAPI

LLC tumor

IgG

15C4

PD-1

15C4 + PD-1

Supplemental Figure 7

Supplemental Figure 1. *Lrg1* is minimally expressed in normal tissue but is highly expressed in the liver. RNAScope® *in situ* hybridization of sections from wild-type (non-tumor bearing) mouse tissue showing skin, pancreas and normal intestine, do not express *Lrg1*. Positive control transcript *Ppib* (**A**) or *Lrg1* (**B**) signal and immunohistochemical staining of endothelial cells (CD31). Scale bar, 100 µm. (**C**) Schematic illustration of LLC spontaneous metastasis model, in which mice develop lung metastases following primary tumor resection. (**D**) RNAScope® *in situ* hybridization for *Lrg1* in sections of wild type mouse liver (positive control), *Lrg1*-/- mouse liver, and normal lung counterstained with antibodies against ERG and podocalyxin showing negative *Lrg1* expression in normal mouse lung. DAPI shown in blue. Region in hashed box enlarged on the right and split into separate channels. Scale bar, 50 µm.

Supplemental Figure 2. **Effect of *Lrg1* knockout or LRG1 inhibition on tumor growth and vascular structure.** Individual growth curves (from data shown in Figure 2A,B) for B16-F0 (**A**) and LLC (**B**) subcutaneous tumors from *Lrg1*+/+ or *Lrg1*-/- mice. Immunohistochemical staining for tumor vascular density (**C**) and association with basement membrane (**D**) in colorectal cancer models. (**C**) CD31 stained sections of the vasculature from *Apc*^Min/+ and *vil*^CreER *Apc*^fl/+ adenomas from *Lrg1*+/+ and *Lrg1*-/- mice. Scale bar, 50 µm. (**D**) Endothelial basement membrane association with tumor vessels in sections labelled with antibodies to CD31, perlecan and/or collagen IV. Scale bar, 100 µm. (**E**). Individual growth curves of data shown in Figure 4A of B16-F0 tumors from wild-type mice treated with control antibody (IgG) or anti-LRG1 (15C4) (mean ± 95% CI). IgG, *n*=35 mice; 15C4, *n*=39 mice. RM two-way ANOVA. (**F**). Vascularity of B16-F0 tumors from WT mice treated with control antibody (IgG) or anti-LRG1 (15C4) revealed by CD31 immunohistochemistry. Scale bar, 250 µm. Graphs show percentage of CD31+ area in the image, and vessel density and cross-sectional area of individual CD31+ objects (mean ± 95% CI). IgG, *n*=14 tumors; 15C4, *n*=18 tumors. Mann Whitney test. *P<0.05, ****P<0.0001. (**G**) Endothelial basement membrane association with tumor vessels from wild-type mice treated with IgG or 15C4. Sections were labelled with antibodies to CD31, perlecan and/or collagen IV. Scale bar, 100 µm. Overlap with endothelium was measured and normalized to mean control value in each experiment (mean ± sem). IgG *n*=12, 15C4 *n*=13.

Supplemental Figure 3. **Expression of genes associated with vascular function.** Differential expression of key genes involved in vascular maturation or destabilization identified by RNASeq analysis. Genes are grouped into families and expressed as fold change in whole B16-F0 tumors in *Lrg1*-/- mice compared to tumors from *Lrg1*+/+ mice. N=3 for each group. (**A**) or from B16-F0 tumor vessel endothelial cells isolated from wild type mice treated with anti-LRG1 antibody 15C4 compared to control IgG treated animals. N=3 for each group. (**B**). P-value adjusted for multiple testing using the Benjamini-Hochberg method. *$P < 0.05$.

Supplemental Figure 4. **Effect of LRG1 inhibition on TGFβ associated signaling pathways and adhesion molecules.** Western blot analysis for phosphorylated signaling components associated with non-canonical (**A**) and canonical (**B**) TGFβ signaling pathways. GAPDH was used as a sample integrity control. Bar graphs show the densitometric analysis of the ratio of phosphorylated to total proteins after normalization to GAPDH (N≥5 per group). Non-parametric unpaired t-test. *P<0.05, **P<0.01. (**C**) Gene expression of key endothelial cell adhesion molecules involved in leukocyte recruitment in B16-F0 tumors from *Lrg1*^{-/-} mice compared to wild type controls. N=3 per group. RNASeq data expressed as fold change.

Supplemental Figure 5. B16-F0 tumor growth curves from individual mice treated with cisplatin or adoptive T cells alone or in the presence of LRG1 blocking antibody 15C4. (**A**) Individual B16-F0 tumor growth rates in mice treated with IgG, 15C4, IgG plus cisplatin or 15C4 plus cisplatin (from mean data shown in Figure 5A). (**B**) Individual NP68-expressing B16-F10 tumor growth rates (from data shown in Figure 6A) of untreated mice or mice treated with control IgG, 15C4, IgG plus adoptive F5B6 cytotoxic T cells or 15C4 plus F5B6 T cells.

Supplemental Figure 6. B16-F0 tumor growth curves from individual mice treated with adoptive T cells or anti-PD1 alone or in the presence of LRG1 blocking antibody 15C4. (**A**) Individual growth curves of tumors (from Fig 6D) from mice bearing NP68-expressing B16-F10 subcutaneous tumors treated with F5B6 cytotoxic T cells and 15C4. (**B**) Immunohistochemical detection of CD3+ and donor T cell (CD90.2) infiltration into NP68-expressing B16-F10 subcutaneous tumors from mice treated with adoptive T cells alone or a combination of adoptive T cells and 15C4. Scale bar, 1 mm. (**C**) Individual growth curves of tumors (from Figure 7A) from mice bearing B16-F0 subcutaneous tumors and treated with IgG control, IgG plus 15C4, IgG plus anti-PD1 and 15C4 plus anti-PD1.

Supplemental Figure 7. Effect of LRG1 inhibition on LLC tumor growth and immune cell infiltration and on B1-F0 HEV formation. A) Mean growth curves of LLC subcutaneous tumors from wild type mice treated with control IgG (n=34) 15C4 (n=32), anti-PD1 (n=32) and 15C4 plus anti-PD1 (n=32) (mean ± S.E.M). Growth curves analyzed by linear regression comparing pairs as shown, *P<0.05, **P<0.01, ****P<0.0001. (**B**) CD3+ and granzyme B+ T cell infiltration of LLC tumors. Scale bar 150 µm. Graphs show density (objects/mm^2) of CD3+ T cells (**C**) and granzyme B (**D**) from the different LLC treatment arms. Student t-test, *P<0.05, **P<0.01. (**E**) qPCR analysis of fold change in HEV signature genes in B16-F0 tumors from mice treated with control IgG, 15C4 plus IgG, anti-PD1 antibody and a combination of 15C4 and anti-PD1. N ≥ 3 samples per group. (**F**) Immunohistochemical staining of lymph node and B16-F0 tumors with an anti-CD31 antibody and the MECA79 antibody to detect PNAd. Tumors were taken from mice treated with control IgG, 15C4, anti-PD1 antibody and a combination of 15C4 and anti-PD1. Scale bar 50 µm.(**G**) Immunohistochemical staining of LLC tumors as in **F** above from mice treated with control IgG, 15C4, anti-PD1 antibody and a combination of 15C4 and anti-PD1. Scale bar 50 µm.